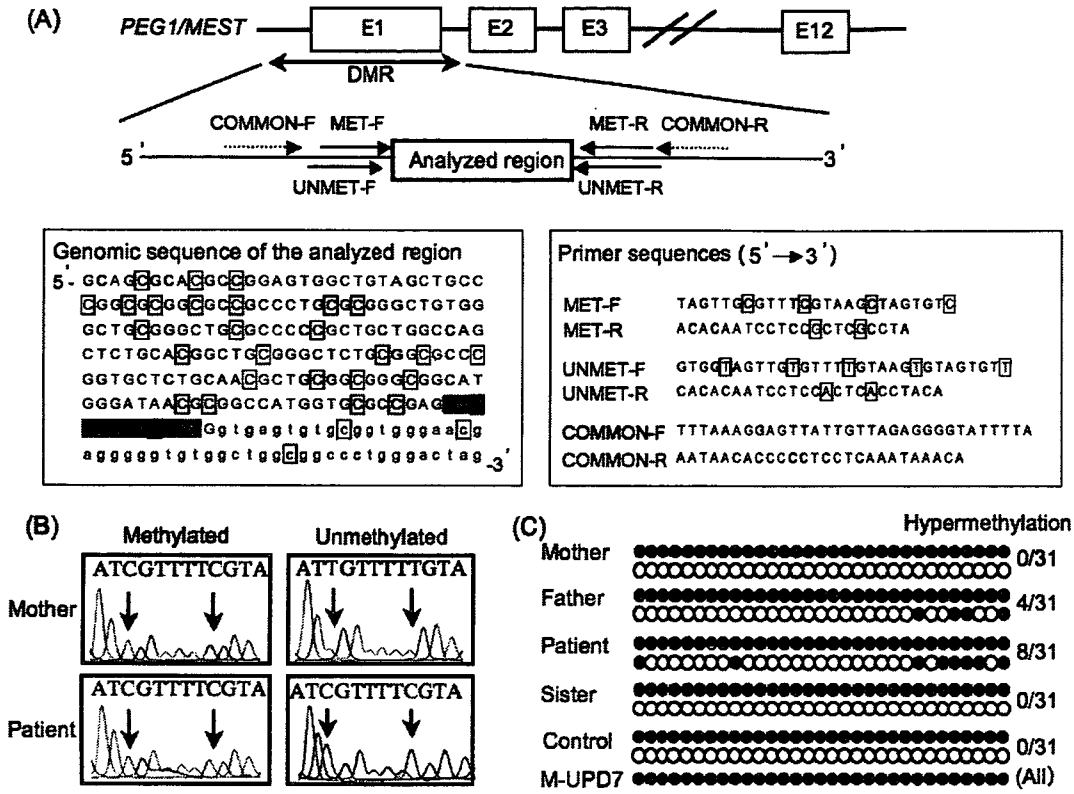

Fig. 2 Methylation analysis of the *PEG1/MEST*-DMR (differentially methylated region). (A) Methylation pattern analysis employed in the present study. The upper part: a schematic representation indicating the analyzed region within the DMR encompassing E1 (exon 1) of *PEG1/MEST*. The positions of the primers utilized for the polymerase chain reaction (PCR) are also shown. The lower left part: genomic sequence of the analyzed region containing 31 CpG dinucleotides. The cytosine residues surrounded by squares are methylated on the maternally derived alleles and unmethylated on the paternally derived alleles. The shaded nucleotide sequence is shown in the electrochromatograms. The lower right part: primer sequences utilized in this study. MET-F and MET-R are designed to hybridize the sequence harboring cytosines, so that they specifically amplify the maternally derived alleles with methylated cytosines at the CpG dinucleotides after bisulphite treatment. UNMET-F and UNMET-R are designed to hybridize the sequence harboring thymines, so that they specifically amplify the paternally derived alleles with thymines converted from unmethylated cytosines via uracils after bisulphite treatment. The nucleotides specific to the methylated and unmethylated alleles are surrounded by squares. COMMON-F and COMMON-R are designed to hybridize the sequence lacking CpG dinucleotides, so that they amplify both paternally and maternally derived alleles after bisulphite treatment. (B) Representative electrochromatograms of a region containing two CpG dinucleotide sequences obtained after bisulphite treatment. The cytosines at the CpG nucleotides are delineated as cytosines (arrows) in the PCR products obtained with MET-F and MET-R (Methylated) in the mother and the patient. In the PCR products obtained with UNMET-F and UNMET-R (Unmethylated), the cytosines at the CpG nucleotides are detected as thymines in the mother and as cytosines in the patient (arrows). (C) Summary of the methylation status of the cytosine residues at the 31 CpG dinucleotides examined after bisulphite treatment. The black circles represent cytosine residues, and the open circles denote thymine residues. The sequence results obtained with MET-F and MET-R are shown on the upper array of circles, and those obtained with UNMET-F and UNMET-R are indicated on the lower array of circles. Hypermethylation, as indicated by the presence of cytosine residues in the PCR products obtained with UNMET-F and UNMET-R, has been identified in 4 of the 31 cytosines in the father and in 8 of the 31 cytosines in the patient. In a subject with maternal disomy for chromosome 7, the PCR products have been obtained only with MET-F and MET-R, and cytosines only have been delineated. The methylation pattern is normal in the mother and the sister, as well as in control subjects

budding, and her height was 128.7 cm (− 0.3 SD), weight 24.7 kg (− 0.8 SD), and HC 51.9 cm (− 0.5 SD).

One and half years after the birth of the twins, a younger son with normal phenotype was born after natural conception.

Methylation analysis

This study has been approved by the Institutional Review Board Committee at National Center for Child Health and Development. Methylation pattern was first analyzed for the DMR of *PEG1/MEST*, using leukocyte genomic DNA of the twins and the parents (Fig. 2A). In brief, after bisulphite treatment that converts all the cytosines except for methylated cytosines at the CpG islands into uracils and subsequently thymines [13], a genomic sequence containing 31 CpG dinucleotides was amplified by polymerase chain reaction (PCR) with a methylated allele specific primer pair (MET) hybridizing to a region containing unconverted methylated cytosines and an unmethylated allele specific primer pair (UNMET)

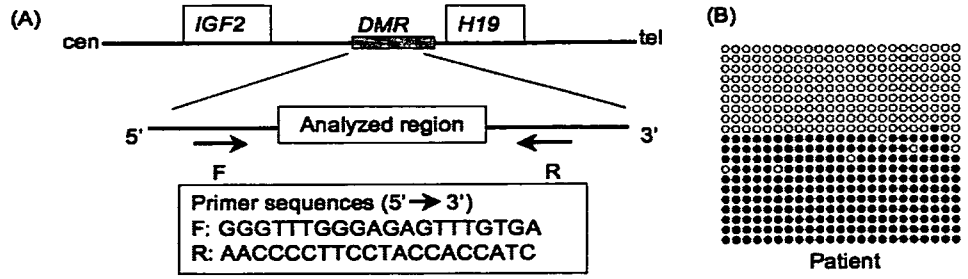

Fig. 3 Methylation analysis of the *H19*-DMR (differentially methylated region). (A) A schematic representation indicating the analyzed region. PCR was performed after bisulphite treatment with the primers that amplify both the methylated and unmethylated alleles. (B) The results of methylation analysis. Each lane indicates a single cloned allele, and each circle denotes a CpG island; filled and open circles represent methylated and unmethylated cytosines, respectively. Both of the methylated and unmethylated alleles are identified with a similar frequency in the patient

hybridizing to a region containing thymines converted from unmethylated cytosines [14]. Subsequently, the PCR products were subjected to direct sequencing on a CEQ 8000 autosequencer (Beckman Coulter, Fullerton, CA). Since maternally derived cytosines at the CpG dinucleotides are normally methylated, they should appear as cytosines in the PCR products obtained with MET; conversely, since paternally derived cytosines at the CpG dinucleotides are normally unmethylated, they should be detected as thymines in the PCR products obtained with UNMET. Furthermore, sequencing analysis was also performed with another primer pair (COMMON) that hybridizes to a region lacking CpG dinucleotides [15]. Since PCR with COMMON amplifies both methylated and unmethylated alleles, cytosines at the CpG dinucleotides are normally delineated as heterozygous peaks for cytosines and thymines after bisulphite treatment. For a control, the DNA samples of a previously described SRS patient with mUPD7 [14] and 50 normal subjects were similarly examined with permission.

Next, methylation analysis was performed for the *H19*-DMR which is methylated after paternal transmission and unmethylated after maternal transmission (Fig. 3A). In brief, after the bisulphite treatment, a 319 bp sequence containing 23 CpG dinucleotides was amplified with primers that hybridize to a region lacking CpG dinucleotides. Subsequently, the PCR products were subcloned with TOPO TA Cloning Kit (Invitrogen, Carlsbad, CA), and 20 clones were subjected to direct sequencing.

Furthermore, methylation status was similarly analyzed for a genomic sequence containing 10 CpG dinucleotides within the DMR of *SNRPN* (small nuclear ribonucleoprotein polypeptide N) on 15q11.2, where cytosines at the CpG dinucleotides are unmethylated on the paternally derived allele and methylated on the maternally derived allele [13, 16].

Microsatellite analysis

Microsatellite analysis was performed for 14 loci widely dispersed on chromosome 7. In brief, leukocyte genomic DNA of the twins and the parents was amplified by PCR with fluorescently labeled forward primers and unlabeled reverse primers, and the PCR products were determined for the fragment size on an ABI PRISM 310 autosequencer using GeneScan software (Applied Biosystems, Perkin Elmer, Foster City, CA). The primer sequences were as described in Genome Database (http://www.gdb.org/).

Results

Methylation analysis

The results of the *PEG1/MEST*-DMR are shown in Fig. 2B and C. In the patient and the father, while all the 31 cytosines at the CpG dinucleotides were detected as cytosines in the PCR products amplified with MET, eight of the 31 cytosines in the patient and four of the 31 cytosines in the father were found to be cytosines, not thymines, in the PCR products amplified with UNMET. In the mother and the sister as well as in the 50 control subjects, all the 31 cytosines at the CpG dinucleotides were delineated as cytosines and thymines in the PCR products amplified with MET and UNMET, respectively. In the SRS patient with mUPD7, PCR products were obtained only with MET, and all the 31 cytosines at the CpG dinucleotides were detected as cytosines. The sequences of the PCR products with COMMON confirmed the results, and showed the absence of abnormal methylation in the MET and UNMET hybridizing region.

The results of the *H19*-DMR are indicated in Fig. 3B. The methylated and the unmethylated alleles were delineated with a similar frequency in the patient. The methylation pattern of the DMR at *SNRPN* was also normal (data not shown).

Microsatellite analysis

Genotyping results were consistent with biparental origin of the chromosome 7 in the patient as well as in the twin sister

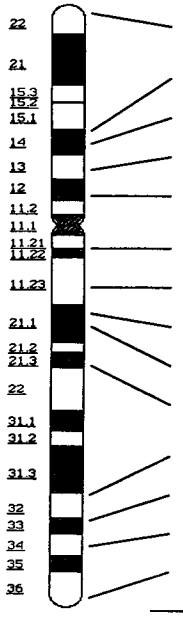

Locus	Product size (bp)			
	Patient	Sister	Father	Mother
D7S531	245/249	N.E.	245/249	245/247
D7S484	99/101	N.E.	101/105	97/99
D7S2846	169/185	177/185	169/177	185/189
D7S519	260/262	N.E.	260/262	260/262
D7S1830	204/212	N.E.	208/212	204/208
D7S672	133/151	131/151	131/133	135/151
D7S1870	107/119	107/117	117/119	107/121
D7S669	118/126	118/130	126/130	118/126
D7S634	139	137/139	137/139	137/139
D7S527	271/279	N.E.	271/275	279/295
D7S515	157/161	155/161	155/157	151/161
D7S684	168/180	168/184	180/184	168/180
D7S1824	169	N.E.	169/173	169/173
D7S550	188/200	N.E.	188/200	186/188

Fig. 4 Summary of microsatellite analysis. The ideogram of chromosome 7 is shown with the cytogenetic localization of the microsatellite loci examined. The locus position is based on Ensembl Human Genome Browser (http://www.ensembl.org). N.E.: not examined

(Fig. 4). Furthermore, the genotype comparison between the twins indicated that, for six of the seven loci examined in the sister, the twins inherited different alleles from the father and the same allele from the mother, although the results of *D7S634* were not informative. In particular, the paternal origin of the alleles for *D7S515* and *D7S684* flanking *PEG1/MEST* was different between the twins.

Discussion

The present study revealed a partial hypermethylation (8/31) at the examined DMR of *PEG1/MEST* in the patient. Furthermore, four of the eight abnormally methylated cytosines were also identified in the father, and the microsatellite analysis indicated the different paternal allelic origin of *PEG1/MEST* between the twins. It is inferred, therefore, that the paternal *PEG1/MEST* allele with mildly hypermethylated DMR was further methylated and transmitted to the patient. Although the mechanism leading to such enhanced methylation remains to be clarified, it may be due to some environmental factor(s) inherent to IVF such as *in vitro* culture or media used, or to some genetic factor(s) relevant to the mild hypermethylation in the father that may also be involved in the subfertility in this couple [17]. In this regard, this girl was conceived by simple mixture of sperms and oocytes, whereas most patients with Beckwith-Wiedermann syndrome and Angelman syndrome with loss of imprinting of maternally imprinted genes such as *LIT1* (long QT intronic transcript 1) as well as a single SRS patient with hypomethylated *H19*-DMR have been conceived by ISCI [8–12, 17]. Such technical difference might underlie the partial hypermethylation in this patient.

It is uncertain whether the partial hypermethylation is relevant to the development of SRS in this patient. However, hypomethylation of the *H19*-DMR was excluded, and the partial hypermethylation might have affected the expression of *PEG1/MEST*, contributing to the SRS phenotype. In support of this, while no *PEG1/MEST* mutation has been identified in patients with SRS [15], *Peg1/Mest* knockout mice show pre- and post-natal growth failure when the mutant gene is transmitted from the father [18]. In addition, while it is unlikely that such abnormal methylation has occurred in multiple DMRs, as indicated by the normal methylation pattern of the *SNRPN*-DMR, it might be possible that such abnormal methylation is also present in other DMRs of the imprinted gene(s) for SRS, impairing the expression of the corresponding gene(s). In this regard, methylation pattern was not examined for the DMR region of *GRB10*, because *GRB10* shows biparental expression in most tissues, except for the brain in which the paternally derived allele is preferentially expressed [19].

The results, though fragmentary, would provide a new insight into the genetic mechanism(s) for the development of LBW in individuals conceived by ART. The mUPD7 results in growth failure with and without SRS phenotype [20]. Furthermore, paternally expressed genes usually serve to promote fetal growth, and maternal disomy for several chromosomes are known to cause growth failure [20]. Thus, excessive methylation affecting the expression of paternally expressed gene(s) including *PEG1/MEST* may be involved in the high prevalence of LBW in individuals born after ART. In this context, while loss of imprinting of maternally imprinted genes and resultant overexpression of paternally expressed genes have been identified in most of the patients born after ART who have Beckwith-Wiedermann syndrome and Angelman syndrome associated with normal to relative excessive growth [17] as well as in ART-related large offspring syndrome in ruminants [21], hypermethylation of paternally expressed genes has not been studied in LBW patients conceived by ART. Thus, methylation pattern in paternally expressed genes would be worth analyzing in such patients.

In summary, we observed partial hypermethylation in an SRS girl conceived with use of ART. Further studies will serve to clarify the relevance of abnormal imprinting to the high prevalence of LBW with and without SRS phenotype in subjects born after ART.

Acknowledgements This work was supported by a grant for Child Health and Development (17C-2) and a grant for Research on Children and Families from the Ministry of Health, Labor, and Welfare.

References

1. Hitchins MP, Stanier P, Preece MA, Moore GE: Silver-Russell syndrome: A dissection of the genetic aetiology and candidate chromosomal regions. J Med Genet 2001;38:810–9.
2. Preece MA, Abu-Amero SN, Ali Z, Abu-Amero KK, Wakeling EL, Stanier P, Moore GE: An analysis of the distribution of hetero- and isodisomic regions of chromosome 7 in five mUPD7 Silver-Russell syndrome probands. J Med Genet 1999;36:457–60.
3. Monk D, Wakeling EL, Proud V, Hitchins M, Abu-Amero SN, Stanier P, Preece MA, Moore GE: Duplication of 7p11.2-p13, including GRB10, in Silver-Russell syndrome. Am J Hum Genet 2000;66:36–46.
4. Hannula K, Lipsanen-Nyman M, Kontiokari T, Kere J: A narrow segment of maternal uniparental disomy of chromosome 7q31-qter in Silver-Russell syndrome delimits a candidate gene region. Am J Hum Genet 2001;68:247–53.
5. Gicquel C, Rossignol S, Cabrol S, Houang M, Steunou V, Barbu V, Danton F, Thibaud N, Le Merrer M, Burglen L, Bertrand AM, Netchine I, Le Bouc Y: Epimutation of the telomeric imprinting center region on chromosome 11p15 in Silver-Russell syndrome. Nat Genet. 2005;37:1003–7.
6. Hansen M, Kurinczuk JJ, Bower C, Webb S: The risk of major birth defects after intracytoplasmic sperm injection and in vitro fertilization. N Engl J Med 2002;346:725–30.
7. Schieve LA, Meikle SF, Ferre C, Peterson HB, Jeng G, Wilcox LS: Low and very low birth weight in infants conceived with use of assisted reproductive technology. N Engl J Med 2002;346:731–37.
8. Cox GF, Burger J, Lip V, Mau UA, Sperling K, Wu BL, Horsthemke B: Intracytoplasmic sperm injection may increase the risk of imprinting defects. Am J Hum Genet 2002;71:162–64.
9. DeBaun MR, Niemitz E, Feinberg AP: Association of in vitro fertilization with Beckwith-Wiedemann syndrome and epigenetic alterations of LIT1 and H19. Am J Hum Genet 2003;72:156–60.
10. Gicquel C, Gaston V, Mandelbaum J, Siffroi JP, Flahault A, Le Bouc Y: In vitro fertilization may increase the risk of Beckwith-Wiedemann syndrome related to the abnormal imprinting of the KCN1OT gene. Am J Hum Genet 2003;72:1338–41.
11. Maher ER, Brueton LA, Bowdin SC, Luharia A, Cooper W, Cole TR, Macdonald F, Sampson JR, Barratt CL, Reik W, Hawkins MM: Beckwith-Wiedemann syndrome and assisted reproduction technology (ART). J Med Genet 2003;40:62–64.
12. Bliek J, Terhal P, Van Den Bogaard MJ, Maas S, Hamel B, Salieb-Beugelaar G, Simon M, Letteboer T, Van Der Smagt J, Kroes H, Mannens M: Hypomethylation of the H19 gene causes not only Silver-Russell syndrome (SRS) but also isolated asymmetry or an SRS-like phenotype. Am J Hum Genet 2006;78:604–14.
13. Kubota T, Das S, Christian SL, Baylin SB, Herman JG, Ledbetter DH: Methylation-specific PCR simplifies imprinting analysis. Nat Genet 1997;16:16–17.
14. Kosaki K, Kosaki R, Robinson WP, Craigen WJ, Shaffer LG, Sato S, Matsuo N: Diagnosis of maternal uniparental disomy of chromosome 7 with a methylation specific PCR assay. J Med Genet 2000;37:E19.
15. Kobayashi S, Uemura H, Kohda T, Nagai T, Chinen Y, Naritomi K, Kinoshita EI, Ohashi H, Imaizumi K, Tsukahara M, Sugio Y, Tonoki H, Kishino T, Tanaka T, Yamada M, Tsutsumi O, Niikawa N, Kaneko-Ishino T, Ishino F: No evidence of PEG1/MEST gene mutations in Silver-Russell syndrome patients. Am J Med Genet 2001;104:225–31.
16. Kosaki K, McGinniss MJ, Veraksa AN, McGinnis WJ, Jones KL: Prader-Willi and Angelman syndromes: diagnosis with a bisulfite-treated methylation-specific PCR method. Am J Med Genet 1997;73:308–13.
17. Niemitz EL, Feinberg AP: Epigenetics and assisted reproductive technology: a call for investigation. Am J Hum Genet 2004;74:599–609.
18. Lefebvre L, Viville S, Barton SC, Ishino F, Keverne EB, Surani MA: Abnormal maternal behaviour and growth retardation associated with loss of the imprinted gene Mest. Nat Genet 1998;20:163–69.
19. Blagitko N, Mergenthaler S, Schulz U, Wollmann HA, Craigen W, Eggermann T, Ropers HH, Kalscheuer VM: Human GRB10 is imprinted and expressed from the paternal and maternal allele in a highly tissue-and isoform-specific fashion. Hum Mol Genet 2000;9:1587–95.
20. Hurst LD, McVean GT: Growth effects of uniparental disomies and the conflict theory of genomic imprinting. Trends Genet 1997;13:436–43.
21. Young LE, Fernandes K, McEvoy TG, Butterwith SC, Gutierrez CG, Carolan C, Broadbent PJ, Robinson JJ, Wilmut I, Sinclair KD: Epigenetic change in IGF2R is associated with fetal overgrowth after sheep embryo culture. Nat Genet 2001;27:153–54.

Clin Pediatr Endocrinol 2007; **16**(4), 99-101

Mutation-in-Brief

KRAS Analysis in 34 Noonan Syndrome Patients without *PTPN11* Mutation

Kaoru Yamamoto[1, 2], Rie Yoshida[1], Tsutomu Ogata[1]

[1]*Department of Endocrinology and Metabolism, National Research Institute for Child Health and Development, Tokyo, Japan*

[2]*Department of Pediatrics, Kyorin University School of Medicine, Tokyo, Japan*

Introduction

Noonan syndrome (NS) is an autosomal dominant disorder characterized by short stature, cardiovascular lesions, and a constellation of minor anomalies including hypertelorism, webbed neck, and cubitus valgus (1). Mental retardation and hearing difficulty are also often observed in affected individuals, as are hypoplastic external genitalia and cryptorchidism in affected males. Furthermore, malignant disorders such as juvenile myelomonocytic leukemia and neuroblastoma have occasionally been reported in NS (2).

Recent molecular studies have successfully revealed genetic causes in NS. It is known that mutations of *PTPN11* (protein-tyrosine phosphatase, nonreceptor type 11) (3), *KRAS* (v-Ki-ras2 Kirsten rat sarcoma viral oncogene homolog) (4, 5), and *SOS1* (son of sevenless homolog 1) (6, 7) account for roughly 45%, <5% and 5–10% of NS patients, respectively, although the underlying genetic factors are still unknown in a substantial fraction of NS patients. Since such genes are involved in the mitogen-activated protein kinase signaling pathway, this explains the occasional occurrence of malignant disorders in NS (2). Here, we report mutation analysis of *KRAS* in *PTPN11* mutation negative NS patients.

Received: June 19, 2007
Accepted: September 4, 2007
Correspondence: Dr. Tsutomu Ogata, Department of Endocrinology and Metabolism, National Research Institute for Child Health and Development, 2-10-1 Ohkura, Setagaya, Tokyo 157-8535, Japan
E-mail: tomogata@nch.go.jp

Patients and Methods

Patients

This study consisted of 34 NS patients (22 males and 12 females) aged 0.1–34.5 years who met the diagnostic criteria proposed by van der Burgt *et al.* (8). All patients were found to have no discernible mutations in the coding exons 1–15 of *PTPN11* by direct sequencing; the clinical and molecular data in *PTPN11* mutation positive patients have been reported previously (9). The karyotype was normal in all the patients.

Mutation analysis of *KRAS*

This study was approved by the IRB at the National Center for Child Health and Development. After obtaining informed consent, leukocyte genomic DNA of each patient was amplified by PCR for all the 5 exons (exons 1–4b) and their flanking splice sites of the *KRAS* gene (isoforms A and B). Subsequently, the PCR products were subjected to direct sequencing from both directions on a CEQ 8000

Table 1 Primer sequences, product sizes and annealing temperatures

	Forward primer Reverse primer	PS AT
Exon 1	GGTGGAGTATTTGATAGTGTATTAACC	246
	AATGGTCCTGCACCAGTAATATG	58
Exon 2	TCTTTGGAGCAGGAACAATG	402
	TGCATGGCATTAGCAAAGAC	58
Exon 3	TGACAAAAGTTGTGGACAGG	391
	AGAAGCAATGCCCTCTCAAG	58
Exon 4a	CAAACTTCTTGCACATGGCTTTCCC	298
	CACCTAAGTAGTTCTAAAGTGGTTGCC	58
Exon 4b	CTGTGCCATTGGTTATCCTTGTCTTTTG	488
	GCTAACAGTCTGCATGGAGCAG	58

PS: product size (bp); AT: annealing temperature (C).

autosequencer (Beckman Coulter, http://www.beckman.com/). The primer sequences and PCR conditions are shown in Table 1.

Results

No mutations were identified in any of the patients, while the previously known silent SNP on exon 4b (519T>C, Asp173Asp, *rs17473423*) was found in 12 patients.

Discussion

No mutations were found in the *KRAS* gene in the 34 NS patients who had no *PTPN11* mutations. This would be consistent with the previous finding that *KRAS* mutations are rare in NS patients (<5%) (2, 4, 5). However, since *KRAS* mutations are frequently associated with malignant lesions (2, 4, 5), *KRAS* appears to be worth analyzing in NS patients.

At present, the underlying genetic cause(s) remains to be clarified in the NS patients examined in this study. Although some of them may have mutations in *SOS1* or in unexamined promoter regions or intronic sequences of *PTPN11* or *KRAS*, most, if not all, of them would be classified as a group of NS patients in whom a causative gene(s) remains to be determined. Thus, when a novel candidate or demonstrated gene for NS has been identified, these patients should be examined for mutations of the gene.

Acknowledgements

This study was supported by grants for Child Health and Development (17C-2) and for Research on Children and Families (H18-005) from the Ministry of Health, Labor, and Welfare of Japan, and by a Grant-in-Aid for Scientific Research on Priority Areas from the Ministry of Education, Culture, Sports and Technology of Japan (16086215 and 1508023).

References

1. Mendez HM, Opitz JM. Noonan syndrome: a review. Am J Med Genet 1985;21:493–506.
2. Tartaglia M, Gelb BD. Noonan syndrome and related disorders: genetics and pathogenesis. Annu Rev Genomics Hum Genet 2005;6:45–68.
3. Tartaglia M, Mehler EL, Goldberg R, Zampino G, Brunner HG, Kremer H, *et al.* Mutations in PTPN11, encoding the protein tyrosine phosphatase SHP-2, cause Noonan syndrome. Nat Genet 2001;29:465–8.
4. Schubbert S, Zenker M, Rowe SL, Boll S, Klein

C, Bollag G, et al. Germline KRAS mutations cause Noonan syndrome. Nat Genet 2006;38:331–6.
5. Carta C, Pantaleoni F, Bocchinfuso G, Stella L, Vasta I, Sarkozy A, *et al.* Germline missense mutations affecting KRAS isoform B are associated with a severe Noonan syndrome phenotype. Am J Hum Genet 2006;79:129–35.
6. Roberts AE, Araki T, Swanson KD, Montgomery KT, Schiripo TA, Joshi VA, *et al.* Germline gain-of-function mutations in SOS1 cause Noonan syndrome. Nat Genet 2007;39:70–4.
7. Tartaglia M, Pennacchio LA, Zhao C, Yadav KK, Fodale V, Sarkozy A, *et al.* Gain-of-function SOS1 mutations cause a distinctive form of Noonan syndrome. Nat Genet 2007;39:75–9.
8. van der Burgt I, Berends E, Lommen E, van Beersum S, Hamel B, Mariman E. Clinical and molecular studies in a large Dutch family with Noonan syndrome. Am J Med Genet 1994;53:187–91.
9. Yoshida R, Hasegawa T, Hasegawa Y, Nagai T, Kinoshita E, Tanaka Y, *et al.* Protein-tyrosine phosphatase, nonreceptor type 11 mutation analysis and clinical assessment in 45 patients with Noonan syndrome. J Clin Endocrinol Metab 2004;89:3359–64.

American Journal of Medical Genetics Part A 146A:514–516 (2008)

Research Letter

Placental Hypoplasia in Maternal Uniparental Disomy for Chromosome 7

Kazuki Yamazawa,[1] Masayo Kagami,[1] Masamichi Ogawa,[2] Reiko Horikawa,[3] and Tsutomu Ogata[1]*

[1]Department of Endocrinology and Metabolism, National Research Institute for Child Health and Development, Tokyo, Japan
[2]Ogawa Clinic Pediatrics and Endocrinology, Nagoya, Japan
[3]Division of Endocrinology and Metabolism, National Center for Child Health and Development, Tokyo, Japan

Received 29 May 2007; Accepted 16 September 2007

How to cite this article: Yamazawa K, Kagami M, Ogawa M, Horikawa R, Ogata T. 2008. Placental hypoplasia in maternal uniparental disomy for chromosome 7. Am J Med Genet Part A 146A:514–516.

To the Editor:

Maternal uniparental disomy for chromosome 7 (mat upd(7)) refers to a condition in which both of the two chromosome 7 homologues are inherited from the mother [Kotzot et al., 2000]. This condition accounts for 7–10% of patients with Silver–Russell syndrome (SRS) characterized by pre- and postnatal growth failure, relative macrocephaly, triangular face, and body asymmetry [Kotzot et al., 2000]. Since maternal heterodisomy as well as isodisomy has been found for all the regions of chromosome 7, and the phenotype is constant in affected individuals, it seems likely that an imprinted gene(s), rather than the unmasking of a recessive allele by isodisomy, is the cause of the SRS phenotype [Preece et al., 1999]. Furthermore, molecular studies in key patients have suggested two separate critical regions for SRS (7p11.2–p13 and 7q31–qter), and candidate imprinted genes such as *GRB10* at 7p12 and *PEG1/MEST* at 7q32.2 have been identified, together with *PEG10* at 7q21 [reviewed in Hitchins et al., 2001]. In addition, loss of the paternal allele of *FOXP2* at 7q31 could be relevant to language deficits in mat upd(7) patients [Feuk et al., 2006]. However, the gene(s) responsible for the SRS features has not been identified to date.

Imprinted genes are known to play a critical role in placental development [Fowden et al., 2006]. Nevertheless, placental phenotype has been poorly documented in mat upd(7), in contrast to the well described clinical features. Thus, we examined placental weight in three Japanese patients with mat upd(7) (cases 1–3), as well as that of a child born to case 3. This study was approved by the Institutional Review Board Committee at National Center for Child Health and Development, and written informed consent was obtained from each patient or the parent(s).

Cases 1–3 were found to have mat upd(7), following molecular studies in 61 Japanese SRS patients. The methods were as described previously [Kosaki et al., 2000; Kagami et al., 2007]. Leukocyte genomic DNA was treated with bisulphite using an EZ DNA methylation kit (Zymo Research, Orange, CA) that converts cytosine except when it is methylated into uracil. Methylation analysis was performed for the differentially methylated region of *PEG1/MEST* using methylated and unmethylated allele-specific PCR primers. Results indicated the presence of only methylated allele of maternal origin in cases 1–3 (Fig. 1A). Subsequently, microsatellite analysis was carried out for nine loci widely dispersed on chromosome 7, showing full maternal isodisomy in cases 1 and 2 and heterodisomy in case 3 (Fig. 1B,C). Microsatellite genotyping was also performed for additional five autosomal loci, confirming the paternity in cases 1–3.

Clinical phenotypes including placental size of cases 1–3 are shown in Table I. Cases 1–3 were born at term, and had pre- and postnatal growth failure and several SRS-compatible features. The placenta was recorded to be small in cases 1–3 with no gross macroscopic abnormalities, although histological findings had not been examined, and there were no preserved placental samples. Oligohydramnios was also noticed during the pregnancy of case 1. Chorionic villus sampling was not performed in cases 1–3. Case 3 gave birth to a male infant with a birth weight of 2.94 kg (−0.1 SD) by a caesarean section at

*Correspondence to: Tsutomu Ogata, M.D., Department of Endocrinology and Metabolism, National Research Institute for Child Health and Development, Tokyo 157-8535, Japan. E-mail: tomogata@nch.go.jp

Published online 17 January 2008 in Wiley InterScience (www.interscience.wiley.com)
DOI 10.1002/ajmg.a.32125

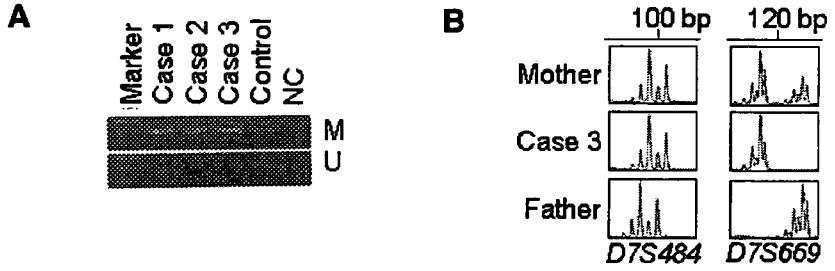

C

Locus	Case 1 Mother	Patient	Father		Case 2 Mother	Patient	Father		Case 3 Mother	Patient	Father	
D7S531	240/250	240	246/246	(I)	246/250	246	244/252	(I)	242	242	242	N.I.
D7S484	99/107	99	101/105	(I)	101	101	97/105	(I)	99/103	99/103	97/101	(H)
D7S2846	177	177	177/181	N.I.	177/181	177	177	N.I.	169/181	169/181	181/185	N.I.
D7S519	255/261	255	263/273	(I)	263/265	265	261/267	(I)	263/265	263/265	263/265	N.I.
D7S672	135/145	145	137/147	(I)	127/145	127	137/143	(I)	131/137	137	127/135	(I)
D7S669	117/119	117	127/131	(I)	127/133	127	125	(I)	117/127	117	127	(I)
D7S684	178/182	182	168/180	(I)	176/180	180	170	(I)	178/180	178/180	176	(H)
D7S1824	165/193	165	173/185	(I)	173/185	185	165/169	(I)	173/185	173/185	169/173	(H)
D7S550	187/191	187	189/191	(I)	187/191	191	189/191	N.I.	187/191	187/191	177/189	(H)

FIG. 1. Results of the molecular studies. **A**: Methylation analysis of the differentially methylated region of *PEG1/MEST*. While PCR products have been produced with both methylated allele-specific primers (M) and unmethylated allele-specific primers (U) in a control subject, they have been obtained only with M in cases 1–3. NC: negative control. **B**: Representative results of microsatellite analysis in case 3. For *D7S484*, both of the maternal alleles are inherited by the patient, whereas both of the paternal alleles are not transmitted to the patient; this demonstrates maternal uniparental heterodisomy for this locus. For *D7S669*, one of the two maternal alleles is transmitted to the patients, and the paternal allele is not inherited by the patient; this confirms maternal uniparental isodisomy for this locus. **C**: Summary of microsatellite analysis in cases 1–3. The Arabic numbers indicate the PCR product sizes in bp. I, isodisomy; H, heterodisomy; and NI, not informative. The results imply maternal isodisomy in cases 1 and 2 and heterodisomy in case 3.

TABLE I. Clinical Features of Cases 1–3 and Two Previously Reported Patients With SRS and Mat Upd(7)

	This study			Previous reports	
	Case 1	Case 2	Case 3	Kotzot et al. [2000]	Miozzo et al. [2001]
Present age (years:months)	4:10	11:09	25:02	10:09	0:05
Sex	Male	Male	Female	Female	Male
Karyotype	46,XY	46,XY	46,XX	46,XX	46,XY
Gestational age (weeks)	39	38	40	36	34
Placental size g (%)[a]	290 (55)	400 (76)	300 (57)	176 (<50)	169 (<50)
Birth length cm (SDS)[b]	47.0 (−1.3)	45.0 (−2.1)	42.5 (−4.1)	40.0 (−2.5)	ND
Birth weight kg (SDS)[b]	2.23 (−2.5)	2.39 (−1.6)	1.97 (−3.3)	1.60 (−2.3)	1.39 (<5 percentile)
Birth OFC cm (SDS)[b]	30.9 (−1.9)	32.5 (−0.5)	32.0 (−0.9)	31.6 (−0.4)	ND
Present height cm (SDS)[c]	91.5 (−3.4)	134.2 (−1.6)[d]	131.3 (−5.0)	128.0 (−2.6)	ND
Present weight kg (SDS)[c]	11.0 (−2.8)	29.8 (−0.9)	27.5 (−3.2)	22.0 (−2.0)	ND
Present OFC cm (SDS)[c]	48.5 (−1.5)	54.1 (−0.1)	54.4 (−0.8)	52.0 (−0.2)	ND
Relative macrocephaly	+	+	+	+	+
Triangular face	+	+	+	+	+
Body asymmetry	+	−	−	ND	+
Clinodactyly V	−	−	−	+	ND
Developmental delay	+	+	−	−	ND
Precocious puberty	NA[e]	+	−	−	NA[e]
Feeding difficulty	+	+	−	+	ND
Paternal age at birth (years)	49	35	27	36	36
Maternal age at birth (years)	35	33	25	39	ND
Paternal height cm (SDS)[c]	170 (−0.1)	166 (−0.8)	171 (±0)	ND	ND
Maternal height cm (SDS)[c]	167 (+1.7)	152 (−1.2)	150 (−1.5)	ND	ND

SRS, Silver–Russell syndrome; mat upd(7), maternal uniparental disomy for chromosome 7; SDS, standard deviation score; OFC, occipitofrontal head circumference; ND, not described; NA, not assessed.

[a]Evaluated by the gestational age-matched Japanese reference data for the placental weight [Nakayama, 2001].

[b]Assessed by the gestational age- and sex-matched Japanese reference data from the Ministry of Health, Labor, and Welfare.

[c]Assessed by the age- and sex-matched Japanese reference data from the Ministry of Health, Labor, and Welfare and from the Ministry of Education, Science, Sports and Culture.

[d]Around −4 SD before the onset of precocious puberty at 8.5 years of age.

[e]Not assessed due to the young age.

38 weeks of gestation; the placental weight was 530 g (101% for the gestational age-matched Japanese reference data) [Nakayama, 2001], and there was no oligohydramnios. At $1\frac{7}{12}$ years of age, the boy had a normal phenotype, with a height of 77.2 cm (−1.4 SD), a weight of 9.45 kg (−1.0 SD), and a head circumference of 47.0 cm (−0.8 SD).

Placental hypoplasia was identified in all the mat upd(7) cases (1–3) born to normal mothers in this report but was absent in the son of case 3 who did not himself have mat upd(7). To our knowledge, although the placenta is rarely discussed in the reports of mat upd(7) cases, placental hypoplasia has been documented in two other mat upd(7) SRS patients (Table I), and there has been no report describing normal placental development in mat upd(7). Of interest, virtually all imprinted genes examined to date are expressed in the placenta and are thought to play an essential role in placental development [Fowden et al., 2006]. Furthermore, although placenta has been poorly studied in patients with uniparental disomy, placentomegaly has been described in several patients with paternal uniparental disomy involving the *IGF2-H19* imprinted domain on 11p15.5 and Beckwith–Wiedemann syndrome [reviewed in Robinson et al., 2007]. These findings, in conjunction with the results of knockout mouse experiments for imprinted genes including *Peg1/Mest* [reviewed in Fowden et al., 2006], point to placental growth, as well as body growth, being promoted by paternally expressed genes and repressed by maternally expressed genes. Thus, placental hypoplasia in cases 1–3 could be primarily ascribed to imprinting due to mat upd(7) in the developing placenta. It should be pointed out, however, that the causes of placental hypoplasia are heterogeneous and may be due to some other genetic or environmental factor(s). In particular, case 3 who was heterodisomic for chromosome 7 could have confined placental mosaicism with trisomy for chromosome 7 [Robinson, 2000], as has been reported before [Kotzot et al., 2000].

It is notable that case 3 gave birth to a normal male infant. This confirms normal reproductive function in females with mat upd(7), and agrees with the predicted model of erasure and re-establishment of molecular imprinting 'marks' during gametogenesis [Lee et al., 2002]. To our knowledge, one female with mat upd(4) has also produced two children with a normal phenotype [Middleton et al., 2006] and it can be useful for genetic counseling of future patients, to record these events.

REFERENCES

Feuk L, Kalervo A, Lipsanen-Nyman M, Skaug J, Nakabayashi K, Finucane B, Hartung D, Innes M, Kerem B, Nowaczyk MJ, Rivlin J, Roberts W, Senman L, Summers A, Szatmari P, Wong V, Vincent JB, Zeesman S, Osborne LR, Cardy JO, Kere J, Scherer SW, Hannula-Jouppi K. 2006. Absence of a paternally inherited *FOXP2* gene in developmental verbal dyspraxia. Am J Hum Genet 79:965–972.

Fowden AL, Sibley C, Reik W, Constancia M. 2006. Imprinted genes, placental development and fetal growth. Horm Res 65:50–58.

Hitchins MP, Stanier P, Preece MA, Moore GE. 2001. Silver-Russell syndrome: A dissection of the genetic aetiology and candidate chromosomal regions. J Med Genet 38:810–819.

Kagami M, Nagai T, Fukami M, Yamazawa K, Ogata T. 2007. Silver-Russell syndrome in a girl born after in vitro fertilization: Partial hypermethylation at the differentially methylated region of *PEG1/MEST*. J Assist Reprod Genet 24:131–136.

Kosaki K, Kosaki R, Robinson WP, Craigen WJ, Shaffer LG, Sato S, Matsuo N. 2000. Diagnosis of maternal uniparental disomy of chromosome 7 with a methylation specific PCR assay. J Med Genet 37:E19.

Kotzot D, Balmer D, Baumer A, Chrzanowska K, Hamel BC, Ilyina H, Krajewska-Walasek M, Lurie IW, Otten BJ, Schoenle E, Tariverdian G, Schinzel A. 2000. Maternal uniparental disomy 7: Review and further delineation of the phenotype. Eur J Pediatr 159:247–256.

Lee J, Inoue K, Ono R, Ogonuki N, Kohda T, Kaneko-Ishino T, Ogura A, Ishino F. 2002. Erasing genomic imprinting memory in mouse clone embryos produced from day 11.5 primordial germ cells. Development 129:1807–1817.

Middleton FA, Trauzzi MG, Shrimpton AE, Gentile KL, Morley CP, Medeiros H, Pato MT, Pato CN. 2006. Complete maternal uniparental isodisomy of chromosome 4 in a subject with major depressive disorder detected by high density SNP genotyping arrays. Am J Med Genet Part B Neuropsychiatr Genet 141B:28–32.

Miozzo M, Grati FR, Bulfamante G, Rossella F, Cribiu M, Radaelli T, Cassani B, Persico T, Cetin I, Pardi G, Simoni G. 2001. Post-zygotic origin of complete maternal chromosome 7 isodisomy and consequent loss of placental *PEG1/MEST* expression. Placenta 22:813–821.

Nakayama M. 2001. Reference values of placentas and umbilical cords. In: Nakayama M, editor. Placental pathology. Tokyo: Igaku Shoin. p 103–107 (in Japanese).

Preece MA, Abu-Amero SN, Ali Z, Abu-Amero KK, Wakeling EL, Stanier P, Moore GE. 1999. An analysis of the distribution of hetero- and isodisomic regions of chromosome 7 in five mUPD7 Silver-Russell syndrome probands. J Med Genet 36: 457–460.

Robinson WP. 2000. Mechanisms leading to uniparental disomy and their clinical consequences. Bioessays 22:452–459.

Robinson WP, Slee J, Smith N, Murch A, Watson SK, Lam WL, McFadden DE. 2007. Placental mesenchymal dysplasia associated with fetal overgrowth and mosaic deletion of the maternal copy of 11p15.5. Am J Med Genet Part A 143A:1752–1759.

nature genetics

Deletions and epimutations affecting the human 14q32.2 imprinted region in individuals with paternal and maternal upd(14)-like phenotypes

Masayo Kagami[1,20], Yoichi Sekita[2,20], Gen Nishimura[3], Masahito Irie[2], Fumiko Kato[1], Michiyo Okada[1], Shunji Yamamori[4], Hiroshi Kishimoto[5], Masahiro Nakayama[6], Yukichi Tanaka[7], Kentarou Matsuoka[8], Tsutomu Takahashi[9], Mika Noguchi[10], Yoko Tanaka[11], Kouji Masumoto[12], Takeshi Utsunomiya[13], Hiroko Kouzan[14], Yumiko Komatsu[15], Hirofumi Ohashi[16], Kenji Kurosawa[17], Kenjirou Kosaki[18], Anne C Ferguson-Smith[19], Fumitoshi Ishino[2] & Tsutomu Ogata[1]

Human chromosome 14q32.2 carries a cluster of imprinted genes including paternally expressed genes (PEGs) such as *DLK1* and *RTL1* and maternally expressed genes (MEGs) such as *MEG3* (also known as *GTL2*), *RTL1as* (*RTL1* antisense) and *MEG8* (refs. 1,2), together with the intergenic differentially methylated region (IG-DMR) and the *MEG3*-DMR[3–5]. Consistent with this, paternal and maternal uniparental disomy for chromosome 14 (upd(14)pat and upd(14)mat) cause distinct phenotypes[6,7]. We studied eight individuals (cases 1–8) with a upd(14)pat-like phenotype and three individuals (cases 9–11) with a upd(14)mat-like phenotype in the absence of upd(14) and identified various deletions and epimutations affecting the imprinted region. The results, together with recent mouse data[4,8–10], imply that the IG-DMR has an important *cis*-acting regulatory function on the maternally inherited chromosome and that excessive *RTL1* expression and decreased *DLK1* and *RTL1* expression are relevant to upd(14)pat-like and upd(14)mat-like phenotypes, respectively.

Upd(14)pat results in a unique phenotype characterized by facial abnormality, a small, bell-shaped thorax, abdominal wall defects and polyhydramnios[6], and upd(14)mat leads to clinically discernible features such as pre- and postnatal growth failure and early onset of puberty[7]. We identified five individuals with a typical upd(14)pat phenotype (cases 1, 2 and 6–8) and three individuals with a relatively mild upd(14)pat-like phenotype (cases 3–5); we also identified three individuals with a upd(14)mat-like phenotype (cases 9–11), among whom case 11 had severely compromised adult height (**Table 1** and **Supplementary Tables 1–3** online). Cases 1–8 were identified because of the presence of a bell-shaped thorax in the neonatal period (**Supplementary Fig. 1** online), and cases 9–11 were ascertained through familial studies of cases 1–8. Thus, cases 1 and 2 and cases 9 and 10 were identified in the same family (family A), as were case 3 and case 11 (family B) (**Fig. 1**). The remaining cases, 4–8, were sporadic. All karyotypes were normal except for 46,XY,r(14)(p11q32.2) in case 5, and upd(14) was excluded in all cases by microsatellite analysis (**Supplementary Table 4** online).

We examined the 14q32.2 imprinted region (**Fig. 2**) using leukocyte genomic DNA and lymphocyte metaphase spreads of cases 2–11 (case 1 was deceased) and their family members who were willing to participate in this study. We also analyzed blood samples of control subjects and previously reported upd(14)pat and upd(14) mat cases[6,11].

We first determined the DMRs to be examined in this study (**Supplementary Fig. 2a** online). For the IG-DMR[4], *in silico* analysis followed by bisulfite sequencing revealed two DMRs, which we

[1]Department of Endocrinology and Metabolism, National Research Institute for Child Health and Development, Tokyo 157-8535, Japan. [2]Department of Epigenetics, Medical Research Institute, Tokyo Medical and Dental University, Tokyo 101-0062, Japan. [3]Department of Radiology, Tokyo Metropolitan Kiyose Children's Hospital, Tokyo 204-8567, Japan. [4]Mitsubishi Chemical Medience Corporation, Tokyo 174-8555, Japan. [5]Division of Pathology, Saitama Children's Medical Center, Saitama 339-8551, Japan. [6]Division of Pathology, Osaka Medical Center and Research Institute for Maternal and Child Health, Osaka 594-1101, Japan. [7]Divison of Pathology, Kanagawa Children's Medical Center, Yokohama 232-8555, Japan. [8]Division of Pathology, National Center for Child Health and Development, Tokyo 157-8535, Japan. [9]Department of Pediatrics, Akita University School of Medicine, Akita 010-8543, Japan. [10]Department of Neonatology, Chiba Kaihin Municipal Hospital, Chiba 261-0012, Japan. [11]Department of Pediatrics, Tokyo Dental College Ichikawa General Hospital, Ichikawa 272-8513, Japan. [12]Department of Pediatric Surgery, Kyushu University School of Medicine, Fukuoka 812-8582, Japan. [13]Department of Neonatology, Kagoshima City Hospital, Kagoshima 892-8580, Japan. [14]Department of Pediatrics, Takamatsu Red Cross Hospital, Takamatsu 760-0017, Japan. [15]Department of Pediatrics, Numazu City Hospital, Numazu 410-0302, Japan. [16]Division of Medical Genetics, Saitama Children's Medical Center, Saitama 339-8551, Japan. [17]Division of Medical Genetics, Kanagawa Children's Medical Center, Yokohama 232-8555, Japan. [18]Department of Pediatrics, Keio University School of Medicine, Tokyo 160-8582, Japan. [19]Department of Physiology, Development and Neuroscience, University of Cambridge, Cambridge CB2 3EG, UK. [20]These authors contributed equally to this work. Correspondence should be addressed to F.I. (fishino.epgn@mri.tmd.ac.jp) or T.O. (tomogata@nch.go.jp).

Received 21 May 2007; accepted 3 October 2007; published online 6 January 2008; doi:10.1038/ng.2007.56

Table 1 Summary of clinical and molecular findings

	Cases 1[a] & 2	Case 3	Case 4	Case 5	Cases 6–8	Cases 9 & 10	Case 11
Upd(14)pat-like phenotype	+ (typical)	+ (mild)	+ (mild)	+ (mild)	+ (typical)		
Upd(14)mat-like phenotype						+	+ (severe)[b]
IG-DMR	Deleted	Deleted	Deleted	Deleted	Epimutated[c]	Deleted	Deleted
MEG3-DMR	Deleted	Deleted	Deleted	Deleted	Epimutated[c]	Deleted	Deleted
Deleted PEGs	*DLK1*	*DLK1*	*RTL1*	*DLK1*	None	*DLK1*	*DLK1*
		RTL1		*RTL1*			*RTL1*
				DIO3			
Deleted MEGs	*MEG3*	*MEG3*	*MEG3*	*MEG3*	None	*MEG3*	*MEG3*
		RTL1as	*RTL1as*	*RTL1as*			*RTL1as*
		MEG8	*MEG8*	*MEG8*			*MEG8*
Parental origin[d]	Maternal	Maternal	Maternal	Maternal	Maternal	Paternal	Paternal

Detailed clinical features of cases 1–8 and upd(14)pat cases are described in **Supplementary Table 1**, and those of cases 9–11 and upd(14)mat cases are described in **Supplementary Table 2**. Phenotypic assessment is summarized in **Supplementary Table 3**. Chest roentgenograms of cases 1–8 are shown in **Supplementary Fig. 1**.
[a]Case 1, though not studied, presumably has the same deletion as case 2. [b]Adult height is severely compromised in case 11. [c]Hypermethylation of the normally hypomethylated allele of maternal origin (**Fig. 3**). [d]Parental origin of chromosomes with deletions or epimutations. In cases 7, 10 and 11, although parental genotyping data are not informative or available, methylation and FISH analyses indicate hypermethylation of the normally hypomethylated allele of maternal origin in case 7 and loss of the normally hypermethylated allele of paternal origin in cases 10 and 11 (**Fig. 3** and **Fig. 4**).

designated CG4 and CG6. For the *MEG3*-DMR, we confirmed the previously reported DMR[5] (hereafter designated CG7) through bisulfite sequencing and PCR amplification with methylated and unmethylated allele-specific primers.

We then carried out methylation analysis, which showed that the IG-DMR (CG4 and CG6) and the *MEG3*-DMR (CG7) were severely hypermethylated in cases 2–8, to an extent comparable to that found in the upd(14)pat case, whereas they were grossly hypomethylated in cases 9–11, to a degree similar to that identified in the upd(14)mat case (**Fig. 3** and **Supplementary Fig. 2b**). Notably, we confirmed hypermethylation of normally hypomethylated CG4 clones of maternal origin by informative SNP typing data in cases 6 and 8. We carried out FISH analysis with two long and accurate (LA)-PCR products covering the IG-DMR and the *MEG3*-DMR, and we found familial heterozygous microdeletions in cases from families A and B and a *de novo* heterozygous microdeletion in case 4 (**Fig. 4**). This deletion was also detected in case 5, the individual with the r(14) chromosome, but it was absent in cases 6–8.

Subsequently, we carried out genotyping analysis for 200 loci, showing lack of common alleles for multiple loci between cases 2 and 9 and between cases 9 and 10 in family A, between case 3 and case 11 in family B, between case 4 and the mother, and between case 5 and the mother (**Supplementary Table 4**). We carried out sequencing analyses for LA-PCR products obtained with primers flanking the deleted loci and identified a 108,768-bp deletion involving *DLK1* and *MEG3* in cases 2, 9 and 10 of family A (case 1 presumably had the same deletion), a 411,354-bp deletion involving *WDR25*, *BEGAIN*, *DLK1*, *MEG3*, *RTL1*, *RTL1as* and *MEG8* in cases 3 and 11 of family B, and a 474,550-bp deletion involving *MEG3*, *RTL1*, *RTL1as* and *MEG8* in case 4; in case 5, we carried out FISH analyses with nine BAC probes covering the imprinted region and identified a ~6.5-Mb deletion involving the whole imprinted region (**Fig. 2** and **Supplementary Fig. 3** online). In cases 6–8, we identified neither tiny deletion nor sequence variation around the *DLK1-MEG3* region, including the DMRs and the putative CTCF binding sites[12], by extensive analyses (**Supplementary Fig. 3**), and we found normal methylation patterns for DMRs at the *MEST* promoter[13], the *IGF2-H19* domain[14] and the *SNRPN* promoter[15]. Thus, we determined that cases 6–8 have epimutations affecting the 14q32.2 imprinted region. Although we attempted to examine the expression dosage of the imprinted genes on 14q32.2, expression was absent or extremely faint in leukocytes. The above molecular data from leukocytes are summarized in **Table 1**.

We further examined placental samples, because virtually all the imprinted genes studied to date are expressed in the placenta[16,17]. Using expression analyses combined with SNP genotypings, we confirmed monoallelic paternal expression of *DLK1* and maternal expression of *MEG3* in normal fresh placentas (**Supplementary Fig. 2c**). RT-PCR analyses showed positive PEGs expression and negative MEGs expression in formalin-treated and paraffin-embedded placental samples of cases 2 and 8 and the upd(14)pat case, with *RTL1* expression being obviously elevated in the three placentas compared to a similarly treated control placenta (**Fig. 5a**). Histological examinations showed proliferation of dilated and congested chorionic villi in the three placentas (**Fig. 5b**). Furthermore, CG4 was hypermethylated in the placentas of cases 2 and 8 and the upd(14)pat case and was delineated as the DMR in the control placenta, whereas CG7 was rather hypomethylated in the four placentas and did not show the DMR-compatible methylation patterns (**Supplementary Fig. 2c**).

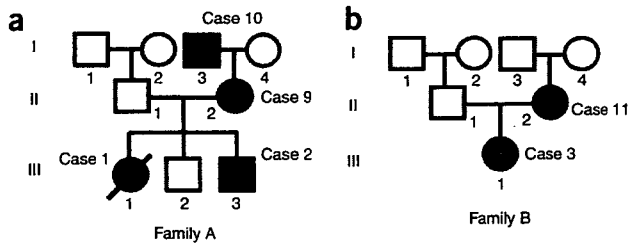

Figure 1 The pedigrees of two families. (**a**) Family A. Case 1 (III-1) and case 2 (III-3) show typical upd(14)pat phenotype (black), whereas case 9 (II-2) and case 10 (I-3) manifest upd(14)mat-like phenotype with mild to moderate short stature (gray). The remaining five family members have normal phenotype. (**b**) Family B. Case 3 (III-1) shows relatively mild upd(14)pat-like phenotype (black), and case 11 has upd(14)mat-like phenotype with marked short stature (gray). The remaining five family members, including the maternal grandparents, have normal phenotype (stature, ± 0 s.d. in the maternal grandfather and –0.8 s.d. in the maternal grandmother). The maternal grandparents refused to take part in molecular studies.

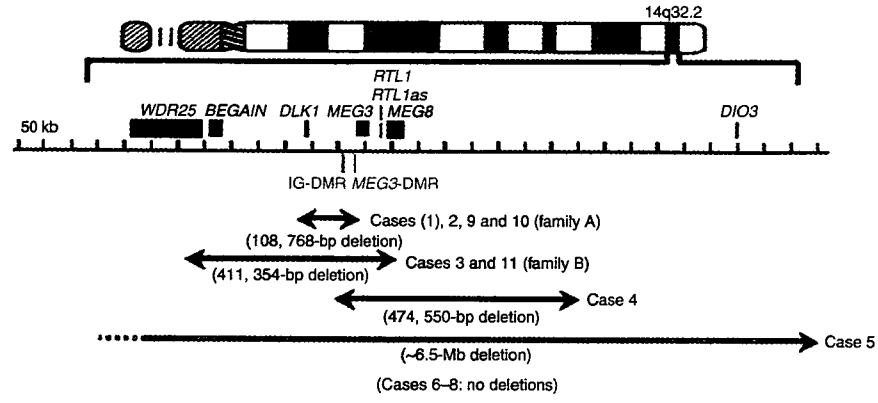

Figure 2 The regional physical map of the human chromosome 14q32.2 imprinted region and the four deletion intervals identified in this study. PEGs are shown in blue and MEGs are shown in red, although it remains to be clarified whether *DIO3* is a PEG; mouse *Dio3* is known to be preferentially but not exclusively expressed from a paternally derived chromosome in embryos[25]. *DAT*[2] (not shown) may also be a PEG in the human, and *Mirg* (*Meg9*)[18] resides between *Rian* (*Meg8*) and *Dio3* in the mouse. *WDR25* and *BEGAIN* seem to be biparentally expressed genes. The two DMRs are depicted in green. The electrochromatograms indicating the fusion points of the three microdeletions are shown in **Supplementary Figure 3**, together with the physical maps representing the deleted regions. The FISH findings identifying the 14q32.2 breakpoint of the r(14) chromosome in case 5 are also shown in **Supplementary Figure 3**. Case 1 of family A was not studied, and no deletion has been identified in cases 6–8.

The human 14q32.2 imprinted region is highly conserved on the distal part of mouse chromosome 12 (ref. 18), in which the germline-derived IG-DMR functions as a *cis*-acting regulator for the imprinted region of maternal origin[4,19]. Targeted deletion of the IG-DMR (ΔIG-DMR) causes paternalization of a maternally derived imprinted region and a unique phenotype comparable to that of paternal uniparental disomy for chromosome 12 (PatDi(12)) in embryos, with ~4.5 times of *Rtl1* expression and ~2 times of *Dlk1* and *Dio3* expression as well as nearly absent expression of MEGs in this imprinted region[4,20,21]. The markedly increased *Rtl1* expression is ascribed to the cumulative effect of the activation of the usually silent maternally derived *Rtl1* and the loss of the microRNA-containing *Rtl1as*, which acts as a repressor for *Rtl1* (refs. 4,9,10). The doubled *Dlk1* and *Dio3* expression is simply a result of the activation of PEGs of maternal origin[4]. The absent MEGs expression is associated with hypermethylation of the *Gtl2*-DMR[4], and this is consistent with the notion that the *Gtl2*-DMR can stay hypomethylated only in the presence of the hypomethylated IG-DMR[4,19]. By contrast, the ΔIG-DMR has no imprinting or clinical effect after paternal transmission[4].

The upd(14)pat-like phenotypes in cases 1–8 are explained by assuming that the human IG-DMR and *RTL1as* have similar functions to the mouse IG-DMR and *Rtl1as*. Indeed, the placental expression data (**Fig. 5a**) are consistent with the deletions and epimutations (hypermethylation) involving the maternally inherited IG-DMR described here, or another yet unidentified IG-DMR(s), resulting in a maternal to paternal epigenotypic alteration with augmented *RTL1* expression. In this case, the excessive *RTL1* expression seems to have a major role in the development of the upd(14)pat-like phenotype, because it is predicted from the mouse data[4,8–10] that cases 3–5, with mild upd(14)pat-like phenotypes, should have moderately increased *RTL1* expression as a result of the presence of a single active copy of *RTL1* in the absence of functional *RTL1as* and that the remaining cases, with typical upd(14)pat phenotypes, should have markedly elevated *RTL1* expression, as in the upd(14)pat cases with two active copies of *RTL1* in the absence of functional *RTL1as* (**Supplementary Table 3**). In support of this, the mouse *Rtl1* is expressed not only in the placenta but also in various fetal tissues including ribs and skeletal muscles[8], and mice with 2.5–3.0 times of *Rtl1* expression caused by maternally derived *Rtl1as* deletion have placental abnormalities[8] similar to those of individuals with the upd(14)pat-like phenotype. By contrast, the typical upd(14)pat phenotype of cases 1 and 2 and the phenotypic similarity between cases 3 and 4 would argue against a

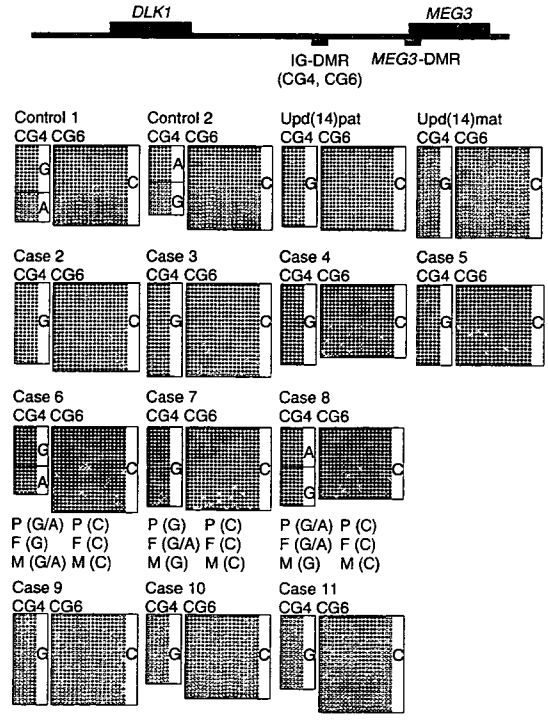

Figure 3 Methylation patterns of the IG-DMR (CG4 and CG6) (those of the *MEG3*-DMR (CG7) are shown in **Supplementary Fig. 2b**). The upper ideogram represents the positions of the IG-DMR and the *MEG3*-DMR. Bisulfite sequencing was done for CG4 and CG6. Each line indicates a single clone, and each circle denotes a CpG island; filled and open circles represent methylated and unmethylated cytosines, respectively. CG4 and CG6 are differentially methylated in control subjects, severely hypermethylated in the upd(14)pat case and cases 2–8 with a upd(14)pat-like phenotype, and grossly hypomethylated in the upd(14)mat case and cases 9–11 with a upd(14)mat-like phenotype. Furthermore, the CG4 SNP typing data (*rs12437020*) are consistent with the parental origin–dependent methylation patterns in the control subjects and show hypermethylation of the maternally derived clones associated with the 'A' allele as well as the paternally derived clones associated with the 'G' allele in case 6 and that of the maternally derived clones associated with the 'G' allele as well as the paternally derived clones associated with the 'A' allele in case 8 (P, patient; F, father; M, mother). The CG6 SNP typing data (*rs10133627*) were not informative. In addition, normal differential methylation patterns were obtained in other examined individuals with a normal phenotype (the father and the maternal grandmother in family A, the father in family B and the parents of cases 4–8) (not shown).

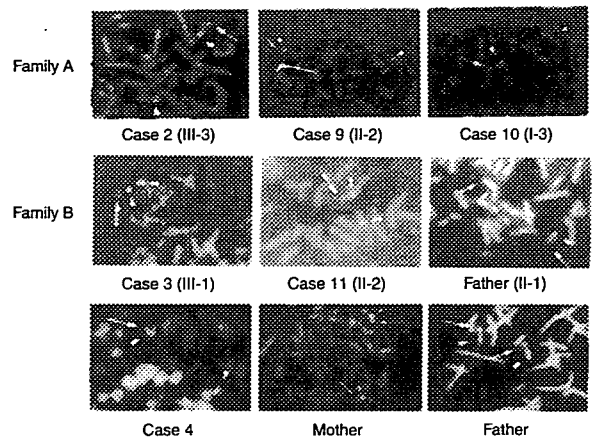

Figure 4 FISH results for the IG-DMR. The red signals (arrows) have been detected by a 5,104-bp LA-PCR product encompassing the CG1–CG6 region (**Fig. 3** and **Supplementary Fig. 2a**), and the green signals (arrowheads) have been identified by an RP11-566I2 probe for 14q12 used as an internal control. Familial heterozygous deletions are identified in cases 2, 9 and 10 of family A and in cases 3 and 11 of family B, and a *de novo* heterozygous deletion is detected in case 4. We also did FISH analyses with a 5,182-bp product encompassing the CG7–CG9 region, showing the same results (not shown).

major role of doubled *DLK1* dosage in the development of upd(14)pat-like phenotype (**Supplementary Table 3**).

The upd(14)mat-like phenotypes of cases 9–11 most likely reflect loss of functional PEGs because it is predicted from the mouse data[4] that deletions involving the paternally derived IG-DMR should not perturb the imprinting status. In this case, loss of active *DLK1* and *RTL1* seems to constitute additive underlying major factors for the development of the upd(14)mat-like phenotype, because a upd(14)mat-like phenotype is common to cases 9–11, who lack active *DLK1*, and growth is more severely compromised in case 11, with additional loss of active *RTL1* (**Supplementary Table 3**). In support of this, the paternally derived *Dlk1* mutation has been previously shown to result in several upd(14)mat-like features, such as pre- and postnatal growth deficiency and obesity and facial abnormalities in mice[22], and the paternally inherited *Rtl1* deletion has been shown to cause mild growth deficiency in mice[8], with the degree of growth failure being ~80% in the two types of knockout mice and ~60% in the MatDi(12) mice lacking functional copies of both *Dlk1* and *Rtl1* (ref. 20). Furthermore, hypomethylation of the paternally inherited DMR adjacent to CG7 has been observed in a single individual with upd(14)mat-like phenotype[23]. This represents a mirror image of epimutations leading to the upd(14)pat-like phenotype and implies that an epimutation is involved in the development of the upd(14)mat-like phenotype.

Although altered *DIO3* and MEGs expression may also be relevant to upd(14)pat/mat phenotypes, the clinical effects would remain minor, if any. Although the primary function of *DIO3* is inactivation of thyroid hormones[24], thyroid dysfunction was absent from cases 1–11 and upd(14)pat/mat cases (this may suggest partial imprinting of human *DIO3*, like that of mouse *Dio3* (ref. 25)) (**Supplementary Tables 1** and **2**). Similarly, although there has been no model mouse with null or doubled MEGs expression that did not show effects on PEGs, *Gtl2*^{lacZ} mice with dysregulated imprinting status caused by a transgene insertion have a normal phenotype with at least 60–80% reduction of all the MEGs[26].

Two findings are noteworthy in reference to the placental studies. First, the methylation profiles of CG4 were similar and those of CG7 were different between leukocytes and placentas of affected and control subjects, as observed in the corresponding regions of normal mice[21]. This implies that the placental imprinting regulation is influenced by the IG-DMR, but is independent of the *MEG3*-DMR, and is also subject to some mechanism(s) such as the control of chromatin conformation[27,28]. Second, phenotypic abnormalities and epigenotypic alterations were identified in the placentas of cases 2 and 8, which had impaired IG-DMRs, whereas they are absent or obscure in the placentas of ΔIG-DMR mice[21]. This suggests that altered gene expression dosage has an essential role in phenotypic development and that there is some difference in IG-DMR function between the human and the mouse placentas (see legend for **Supplementary Fig. 2**).

METHODS

Extraction of DNA and RNA samples. This study was approved by the Institutional Review Board Committee at the National Center for Child Health and Development, and written informed consent was obtained from each subject or his or her parent(s). For leukocytes and fresh placental tissues, we obtained genomic DNA with FlexiGene DNA Kit (Qiagen) and prepared RNA with RNeasy Plus Mini (Qiagen). For paraffin-embedded placental samples, we extracted genomic DNA and RNA with RecoverAll Total Nucleic Acids Isolation Kit (Ambion) using slices of 40 μm thick.

Primers. The primers used in this study are summarized in **Supplementary Table 5** online.

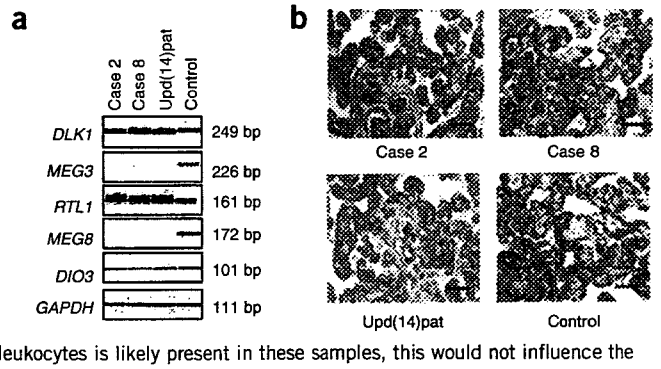

Figure 5 Examinations of placental samples. (**a**) RT-PCR analysis (35–40 cycles) using formalin-treated and paraffin-embedded placental samples of case 2 (30 weeks of gestational age), case 8 (35 weeks), the upd(14)pat case (32 weeks) and a normal subject (33 weeks). *DLK1*, *RTL1* and *DIO3* are expressed and *MEG3* and *MEG8* are not expressed in the placentas of case 2, case 8 and the upd(14)pat case, whereas all the PEGs and MEGs are identified in the control placenta. The results were consistent in RT-PCR experiments performed seven times, except for faint possible *MEG8* expression detected once in the placenta of case 2. Compared to the expression pattern in the control placenta, *RTL1* expression is notably elevated in the placentas of cases 2 and 8 and the upd(14)pat case, and *DLK1* expression is possibly increased in the placentas of case 8 and the upd(14)pat case, although precise quantification was impossible because of poor RNA quality. Although contamination from maternal leukocytes is likely present in these samples, this would not influence the expression pattern, because of absent expression of the imprinted genes in this cell type. (**b**) Histological findings (hematoxylin-eosin staining). The chorionic villi of cases 2 and 8 and the upd(14)pat case are notably proliferated and dilated with congestion, as compared with those of the control subject. The bars represent 100 μm. In addition, nonspecific chorangioma was observed in the placenta of case 2, and interspersed villous calcifications suggestive of degeneration was identified in the placentas of case 8 and the upd(14)pat case.

Genotyping and sequence deletion and variation analyses. Leukocyte genomic DNA was used for these studies. For microsatellite genotyping, we PCR-amplified a segment encompassing each locus with a fluorescently labeled forward primer and an unlabeled reverse primer and determined its size on an ABI PRISM 310 autosequencer using GeneScan software (Applied Biosystems). For polymorphism genotyping, a segment encompassing polymorphism(s) was PCR-amplified and subjected to direct sequencing on a Cequation (8000) autosequencer (Beckman Coulter). For the examination of a tiny deletion and a sequence variation around the *DLK1–MEG3* region, we obtained three LA-PCR products from cases 6–8 and a control subject and subjected them to fragment size comparisons after restriction enzyme digestions and to direct sequencing using serial forward primers (when clear electrochromatograms were not obtained, the corresponding sequences were also analyzed with reverse primers). The three LA-PCR products were a 5,104-bp product encompassing the CG1–CG6 region (also used as FISH probe 1 for the IG-DMR), a 3,142-bp product covering a putative CTCF binding site (A)[12] and a 5,182-bp product encompassing the CG7–CG9 region and six putative CTCF binding sites (B–G)[12] (also used as FISH probe 2 for the *MEG3*-DMR). The restriction enzymes used were *Bam*HI, *Kpn*I and *Nco*I for the 5,104-bp product, *Drd*I and *Taq*I for the 3,142-bp product and *Acl*I, *Eco*RI, *Bss*HII, *Kpn*I and *Sac*I for the 5,182-bp product.

Methylation analysis. Leukocyte and placental genomic DNA were treated with bisulfite using the EZ DNA Methylation Kit (Zymo Research) that converts all the cytosines except for methylated cytosines at the CpG islands into uracils and subsequently thymines. We PCR-amplified the CG1–CG9 regions with primer sets that hybridize to both methylated and unmethylated alleles because of absent CpG dinucleotides within the primer sequences. Then, we subcloned the PCR products with the TOPO TA Cloning Kit (Invitrogen) and subjected multiple clones to direct sequencing on the Cequation (8000) autosequencer. When the PCR products contained SNPs, we also carried out genotyping. For CG7, PCR amplification was also done with a methylated allele-specific primer pair hybridizing to a region containing unconverted methylated cytosines and with an unmethylated allele-specific primer pair hybridizing to a region containing thymines converted from unmethylated cytosines, and the PCR products were subjected to gel electrophoresis, as reported previously[5]. For CG8, combined bisulfite restriction analysis (COBRA) was also carried out using a methylated allele-specific *Hga*I restriction site.

FISH analysis. Lymphocyte metaphase spreads were hybridized with probes for specific sequences at the 14q32.2 imprinted region, together with an RP11-566I2 probe for 14q12 used as an internal control. The FISH probes 1 and 2 were as described above, and FISH probes 3 (5,540 bp) and 4 (6,058 bp) were obtained by LA-PCR for the polymorphism-poor sequences at the *DLK1–MEG3* region. We purchased the nine BAC probes covering the imprinted region from BACPAC Resources Center at Children's Hospital Oakland Research Institute. The probes for specific sequences were labeled with digoxigenin and detected by rhodamine anti-digoxigenin, and the control probe was labeled with biotin and detected with avidin conjugated to fluorescein isothiocyanate.

Expression analysis. We analyzed leukocyte and placental RNA for the expression of PEGs and MEGs on the 14q32.2 region. For the imprinted genes other than *RTL1*, cDNA was synthesized from 1 μg of RNA using Superscript III Reverse Transcriptase (Invitrogen), and RT-PCR was done with 20 ng of total RNA using ExTaq (Takara). For *RTL1*, because the primers hybridizing to exon sequences amplify both *RTL1* and *RTL1as*, we used 3′-RACE. We synthesized cDNA from 1 μg of RNA using Superscript III Reverse Transcriptase with a long primer hybridizing to the poly(A) site and introducing the adaptor sequence, and, subsequently, we carried out RT-PCR for 50 ng of cDNA using KOD Dash (Toyobo) with a primer hybridizing to the adaptor sequence and another primer hybridizing to the exon sequence. The reactions were carried out in 200-μl tubes, and small amounts (1–2 μl) of the reaction solutions were loaded onto Gel-Dye Mix (Agilent) after adjusting the *GAPDH* dosage among examined samples.

To examine monoallelic expression in normal placentas, we subjected placental cDNA and genomic DNA and maternal genomic DNA to direct sequencing with primers designed to amplify regions including exonic SNPs (*rs2295660* for *DLK1*; *rs1884540* for *MEG3*; *rs6575805*, *rs11623267*, *rs35695758*, and *rs12884005* for *RTL1*; *rs11847631* and *rs7159526* for *MEG8*; and *rs11627443* and *rs945006* for *DIO3*).

GenBank accession codes. Genome: NC_000014 for *DLK1*, *MEG3*, *RTL1* and *DIO3*, and AL117190 for *MEG8*; mRNA: NM_003836 for *DLK1*, NR_002766 for *MEG3*, XM_370776 for *RTL1*, CA396130 for *MEG8*, and NM_001362 for *DIO3*.

Note: Supplementary information is available on the Nature Genetics website.

ACKNOWLEDGMENTS

We would like to thank all the affected individuals and their family members who participated in this study. This work was supported by Grants for Child Health and Development (17C-2) and for Research on Children and Families (H18-005) from the Ministry of Health, Labor, and Welfare, and by Grants-in-Aid for Scientific Research (priority areas: 16086215 and 1508023; category B: 19390290) from the Ministry of Education, Culture, Sports, Science and Technology.

AUTHOR CONTRIBUTIONS

Molecular analysis was performed by M.K., Y.S., M.I., F.K., M.O. and S.Y., placental sample collection and preparation by H.K., M.N., Y.T., K.M. and K. Ko., placental pathological examination by K.M., and blood sampling and phenotype assessment by G.N., T.T., M.N., Y.T., K.M., T.U., H.K., Y.K., H.O., K. Ku. and T.O. The study was designed and coordinated by F.I. and T.O. with later input from A.C.F.-S., and the results were interpreted and discussed by A.C.F.-S., F.I. and T.O. The paper was written by T.O.

Published online at http://www.nature.com/naturegenetics
Reprints and permissions information is available online at http://npg.nature.com/reprintsandpermissions

1. Cavaille, J., Seitz, H., Paulsen, M., Ferguson-Smith, A.C. & Bachellerie, J.P. Identification of tandemly-repeated C/D snoRNA genes at the imprinted human 14q32 domain reminiscent of those at the Prader-Willi/Angelman syndrome region. *Hum. Mol. Genet.* **11**, 1527–1538 (2002).
2. Charlier, C. *et al.* Human-ovine comparative sequencing of a 250-kb imprinted domain encompassing the callipyge (*clpg*) locus and identification of six imprinted transcripts: *DLK1, DAT, GTL2, PEG11, antiPEG11*, and *MEG8*. *Genome Res.* **11**, 850–862 (2001).
3. Paulsen, M. *et al.* Comparative sequence analysis of the imprinted *Dlk1-Gtl2* locus in three mammalian species reveals highly conserved genomic elements and refines comparison with the *Igf2–H19* region. *Genome Res.* **11**, 2085–2094 (2001).
4. Lin, S.P. *et al.* Asymmetric regulation of imprinting on the maternal and paternal chromosomes at the *Dlk1-Gtl2* imprinted cluster on mouse chromosome 12. *Nat. Genet.* **35**, 97–102 (2003).
5. Murphy, S.K. *et al.* Epigenetic detection of human chromosome 14 uniparental disomy. *Hum. Mutat.* **22**, 92–97 (2003).
6. Kagami, M. *et al.* Segmental and full paternal isodisomy for chromosome 14 in three patients: narrowing the critical region and implication for the clinical features. *Am. J. Med. Genet. A.* **138**, 127–132 (2005).
7. Kotzot, D. Maternal uniparental disomy 14 dissection of the phenotype with respect to rare autosomal recessively inherited traits, trisomy mosaicism, and genomic imprinting. *Ann. Genet.* **47**, 251–260 (2004).
8. Sekita, Y. *et al.* Role of retrotransposon-derived imprinted gene, *Rtl1*, in the feto-maternal interface of mouse placenta. *Nat. Genet.* advance online publication, doi: 10.1038/ng.2007.51 (6 January 2008).
9. Seitz, H. *et al.* Imprinted microRNA genes transcribed antisense to a reciprocally imprinted retrotransposon-like gene. *Nat. Genet.* **34**, 261–262 (2003).
10. Davis, E. *et al.* RNAi-mediated allelic trans-interaction at the imprinted *Rtl1/Peg11* locus. *Curr. Biol.* **15**, 743–749 (2005).
11. Takahashi, I., Takahashi, T., Utsunomiya, M., Takada, G. & Koizumi, A. Long-acting gonadotropin-releasing hormone analogue treatment for central precocious puberty in maternal uniparental disomy chromosome 14. *Tohoku J. Exp. Med.* **207**, 333–338 (2005).
12. Rosa, A.L. *et al.* Allele-specific methylation of a functional CTCF binding site upstream of *MEG3* in the human imprinted domain of 14q32. *Chromosome Res.* **13**, 809–818 (2005).
13. Kosaki, K. *et al.* Diagnosis of maternal uniparental disomy of chromosome 7 with a methylation specific PCR assay. *J. Med. Genet.* **37**, E19 (2000).
14. Gicquel, C. *et al.* Epimutation of the telomeric imprinting center region on chromosome 11p15 in Silver-Russell syndrome. *Nat. Genet.* **37**, 1003–1007 (2005).
15. Kubota, T. *et al.* Methylation-specific PCR simplifies imprinting analysis. *Nat. Genet.* **16**, 16–17 (1997).
16. Kaneko-Ishino, T., Kohda, T. & Ishino, F. The regulation and biological significance of genomic imprinting in mammals. *J. Biochem.* **133**, 699–711 (2003).

17. Coan, P.M., Burton, G.J. & Ferguson-Smith, A.C. Imprinted genes in the placenta—a review. *Placenta* **26** (Suppl. A), S10–S20 (2005).
18. Kaneko-Ishino, T., Kohda, T., Ono, R. & Ishino, F. Complementation hypothesis: the necessity of a monoallelic gene expression mechanism in mammalian development. *Cytogenet. Genome Res.* **113**, 24–30 (2006).
19. Takada, S. *et al.* Epigenetic analysis of the *Dlk1-Gtl2* imprinted domain on mouse chromosome 12: implications for imprinting control from comparison with *Igf2–H19*. *Hum. Mol. Genet.* **11**, 77–86 (2002).
20. Georgiades, P., Watkins, M., Surani, M.A. & Ferguson-Smith, A.C. Parental origin-specific developmental defects in mice with uniparental disomy for chromosome 12. *Development* **127**, 4719–4728 (2000).
21. Lin, S.P. *et al.* Differential regulation of imprinting in the murine embryo and placenta by the *Dlk1-Dio3* imprinting control region. *Development* **134**, 417–426 (2007).
22. Moon, Y.S. *et al.* Mice lacking paternally expressed Pref-1/Dlk1 display growth retardation and accelerated adiposity. *Mol. Cell. Biol.* **22**, 5585–5592 (2002).
23. Temple, I.K. *et al.* Isolated imprinting mutation of the *DLK1/GTL2* locus associated with a clinical presentation of maternal uniparental disomy of chromosome 14. *J. Med. Genet.* **44**, 637–640 (2007) published online 29 June 2007.
24. Hernandez, A., Martinez, M.E., Fiering, S., Galton, V.A. & St Germain, D.L. Type 3 deiodinase is critical for the maturation and function of the thyroid axis. *J. Clin. Invest.* **116**, 476–484 (2006).
25. Tsai, C.E. *et al.* Genomic imprinting contributes to thyroid hormone metabolism in the mouse embryo. *Curr. Biol.* **12**, 1221–1226 (2002).
26. Sekita, Y. *et al.* Aberrant regulation of imprinted gene expression in *Gtl2*^{lacZ} mice. *Cytogenet. Genome Res.* **113**, 223–229 (2006).
27. Lewis, A. *et al.* Imprinting on distal chromosome 7 in the placenta involves repressive histone methylation independent of DNA methylation. *Nat. Genet.* **36**, 1291–1295 (2004).
28. Umlauf, D. *et al.* Imprinting along the *Kcnq1* domain on mouse chromosome 7 involves repressive histone methylation and recruitment of Polycomb group complexes. *Nat. Genet.* **36**, 1296–1300 (2004).

nature genetics

Role of retrotransposon-derived imprinted gene, *Rtl1*, in the feto-maternal interface of mouse placenta

Yoichi Sekita[1], Hirotaka Wagatsuma[2], Kenji Nakamura[3], Ryuichi Ono[1], Masayo Kagami[4], Noriko Wakisaka[1,5], Toshiaki Hino[3], Rika Suzuki-Migishima[3], Takashi Kohda[1], Atsuo Ogura[6], Tsutomu Ogata[4], Minesuke Yokoyama[3,7], Tomoko Kaneko-Ishino[5] & Fumitoshi Ishino[1]

Eutherian placenta, an organ that emerged in the course of mammalian evolution, provides essential architecture, the so-called feto-maternal interface, for fetal development by exchanging nutrition, gas and waste between fetal and maternal blood. Functional defects of the placenta cause several developmental disorders, such as intrauterine growth retardation in humans and mice. A series of new inventions and/or adaptations must have been necessary to form and maintain eutherian chorioallantoic placenta, which consists of capillary endothelial cells and a surrounding trophoblast cell layer(s)[1]. Although many placental genes have been identified[2], it remains unknown how the feto-maternal interface is formed and maintained during development, and how this novel design evolved. Here we demonstrate that retrotransposon-derived *Rtl1* (retrotransposon-like 1), also known as *Peg11* (paternally expressed 11), is essential for maintenance of the fetal capillaries, and that both its loss and its overproduction cause late-fetal and/or neonatal lethality in mice.

To elucidate *Rtl1* function, we produced knockout (KO) mice (**Supplementary Fig. 1a,b** online). *Rtl1* is a paternally expressed imprinted gene highly expressed at the late-fetal stage in both the fetus and placenta (**Supplementary Fig. 1c**), and it is located in a large imprinted region on distal chromosome 12 (ref. 3; see **Supplementary Table 1** online for imprinting phenotypes[4–6]). Paternally expressed *Rtl1* has an overlapping maternally expressed antisense transcript, *Rtl1* antisense (*Rtl1as*, also known as *antiPeg11*), which contains several microRNAs (miRNAs) targeting the *Rtl1* transcript through an RNAi mechanism[3,7] (**Supplementary Fig. 1a**). We removed the entire Gag- and Pol-like domains of *Rtl1* with approximately 30% homology to the sushi-ichi retrotransposons, together with six of seven miRNAs in *Rtl1as*. Then, we produced two different types of mice: mice with no *Rtl1* expression upon paternal transmission of the KO allele (Pat-KO) and those with 2.5–3.0 times overexpression of the *Rtl1* as a result of deficiency of *Rtl1as* upon maternal transmission (Mat-KO; **Fig. 1a**). We confirmed that the imprinting regulation of distal chromosome 12 was not affected by the KO construct[8,9] (**Supplementary Fig. 1d,e**).

In the course of producing mice with the C57BL/6 (B6) background, we observed that the Pat-KO mice showed pre- and postnatal growth retardation in the F_1 and F_2 generations (**Supplementary Fig. 2a** online), and after the F_3 generation, most showed late-fetal or neonatal lethality (**Fig. 1b,c** and **Supplementary Fig. 3** online). When F_2 males mated with normal B6 females, all the pups, including the wild-type (WT) pups, were born dead as a result of a 3- to 4-d delay of the birth date (**Fig. 1c**; I and II in F_3 generation). When removed by caesarean sections at 19.0 days post coitus (d.p.c.) of the F_3 generation (**Fig. 1c**; III in F_3 generation), the WT pups grew normally, but half of the Pat-KO pups were already resorbing, and the other half were born small (about 80% the weight of the controls) and died by the next day (**Fig. 1c**; III in F_3 generation and **Table 1**). Pat-KO fetuses showed no abnormal phenotypes until 14.5 d.p.c., but half of them died from 15.5 to 19.0 d.p.c. (**Table 1**), and growth retardation of both the fetuses and placentas was observed even in the living half after 15.5 d.p.c. (**Fig. 1d–f**).

In Mat-KO mice, pups, at least after F_2, showed an approximately 15% retardation in growth after weaning (**Supplementary Fig. 2b,c**). Their birth rate gradually diminished after the F_4 generation, and neonatal lethality was predominant in the F_6 generation (**Fig. 1c**, F4–F6; **Supplementary Fig. 3b**, F_4–F_6 and **Supplementary Table 2** online). All the Mat-KO pups reached term normally, with normal weight, but they showed 150% placentomegaly compared to the normal size, and most died within a day (**Fig. 1g,h**). Although the genetic background affected both the Pat-KO and Mat-KO phenotypes to a large degree (**Supplementary Tables 2** and **3** online), these results demonstrate that both the loss and the overproduction

[1]Department of Epigenetics, Medical Research Institute, Tokyo Medical and Dental University, 2-3-10 Kandasurugadai, Chiyoda-ku, Tokyo 101-0062, Japan. [2]Graduate School of Bioscience and Biotechnology, Tokyo Institute of Technology, 4259 Nagatsuta-cho, Midori-ku, Yokohama 226-8501, Japan. [3]Mitsubishi Kagaku Institute of Life Sciences, 11 Minamiooya, Machida, Tokyo 194-8511, Japan. [4]Department of Endocrinology and Metabolism, National Research Institute for Child Health and Development, 2-10-1 Okura, Setagaya-ku, Tokyo 157-8535, Japan. [5]School of Health Sciences, Tokai University, Bohseidai, Isehara, Kanagawa 259-1193, Japan. [6]BioResource Center, RIKEN, 3-1-1 Koyadai, Tsukuba, Ibaraki 305-0074, Japan. [7]Present address: Brain Research Institute, Niigata University, 1-757 Asahimachi-dori, Niigata 951-8585, Japan. Correspondence should be addressed to T.K.-I. (tkanekoi@is.icc.u-tokai.ac.jp) or F.I. (fishino.epgn@mri.tmd.ac.jp).

Received 21 May 2007; accepted 16 October 2007; published online 6 January 2008; doi:10.1038/ng.2007.51

of *Rtl1* interfered with normal fetal development, providing direct evidence for the importance of both retrotransposon-derived *Rtl1* and microRNAs in *Rtl1as*.

Histological analyses demonstrated that severe abnormalities occur in the same place in both the Pat-KO and Mat-KO placentas (that is, the fetal capillaries where the feto-maternal interaction occurs), but the consequences of these abnormalities were different (**Fig. 2**). The mouse placenta consists of three major zones: the decidua basalis, the junctional zone and the labyrinth zone. In the Pat-KO placenta at 15.5 d.p.c., we found abnormal, dark-stained regions in the labyrinth zone upon hematoxylin and eosin (HE) staining (**Fig. 2a**, WT; **b,c**, Pat-KO). Using truidin blue staining and electron microscopy, we confirmed several morphological abnormalities throughout the labyrinth zone, such as splitting of the basement membrane (**Fig. 2d,h**, WT; **e,i**, Pat-KO), the emergence of a number of lysosomes in layer III trophoblast cells (**Fig. 2f,j**) and clogging in the fetal capillaries (**Fig. 2g,k**). When we did immunohistochemical (IHC) staining with CD31, an endothelial cell–specific marker, we observed that its

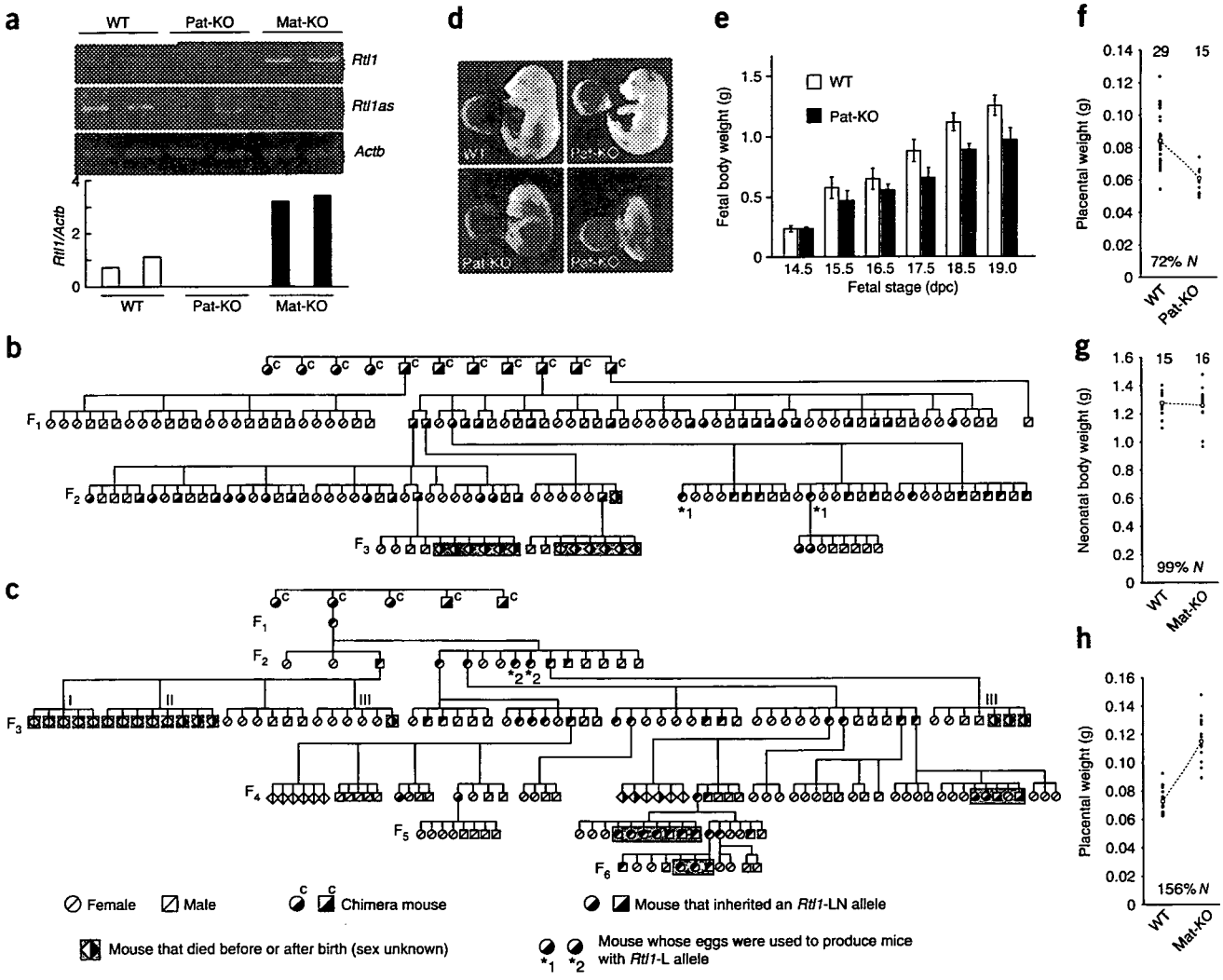

Figure 1 Pedigree of *Rtl1* KO mice. (**a**) Expression of *Rtl1* and *Rtl1as* in WT, Pat-KO and Mat-KO fetuses (*Rtl1*-LN) as determined by RT-PCR. β-actin (encoded by *Actb*) used as a control. The band intensities, measured using ImageJ software are shown below. (**b**) A pedigree from a male chimera. (**c**) A pedigree from a female chimera. A 4-d delay of natural delivery (I) and a caesarean section after a 3-d delay from the expected delivery date (II). All pups were dead in both cases. Caesarean sections were carried out at 19.0 d.p.c. when paternal transmission was analyzed (III). From the F_1 males and females, we obtained many Pat-KO and Mat-KO mice, although the number of Pat-KO mice was slightly smaller than expected from the mendelian ratio (WT/Pat-KO = 24:19, **Supplementary Table 1**) and they grew to adulthood with a reduced body weight (**Supplementary Fig. 2**). Thus, it is clear that the F_1 males and females with the C57BL/6 × 129/Sv F1 (B6/129) genetic background from chimera mice can produce some viable Pat-KO and Mat-KO pups. (**d**) Fetuses at 16.5 d.p.c, including a WT fetus (upper left) and Pat-KO fetuses: small normal-looking (alive) fetus (upper right), pale dead fetus (lower left), and resorbing fetus (lower right). Scale bar, 10 mm. (**e**) Late-fetal growth retardation in Pat-KO fetuses. Open bars, WT fetal body weight; solid bars, Pat-KO fetal body weight. (**f–h**) Growth phenotype of Pat-KO placentas at 18.5 d.p.c. (**f**) and Mat-KO neonates (**g**) and Mat-KO placentas (**h**) at birth (caesarean section). The data in **g** and **h** are from the same litters. Each filled circle represents a single placenta and neonate, respectively. The number at the top represents the total number of weighted samples. Open circles represent average weight. The degree of growth deficiency or promotion of mutant mice is shown as the percentage of WT weight (*N*). Placental and neonatal body weights (mean ± s.d.) are as follows: **f**; WT, 0.085 ± 0.015 ($n = 29$); Pat-KO, 0.061 ± 0.008 ($n = 15$); $P = 1.805 \times 10^{-65}$ (*t*-test), **g**; WT, 1.279 ± 0.087 ($n = 15$); Mat-KO, 1.262 ± 0.126 ($n = 16$), **h**; WT, 0.073 ± 0.009 ($n = 15$); Mat-KO, 0.116 ± 0.016 ($n = 16$); $P = 9.721 \times 10^{-105}$ (*t*-test).

Table 1 Lethality of *Rtl1*-LN (Pat-KO) fetuses and neonates at F_3

Dissection stage (d.p.c.)	WT total	Pat-KO total (dead)	Percentage death in Pat-KO
12.5	5	4 (0)	0
14.5	5	5 (0)	0
15.5	9	7 (1)	14.3
16.5	9	11 (5)	45.5
17.5	10	11 (6)	54.5
18.5	21	24 (13)	54.2
Neonate	35	13 (13)	100

signal diffused to the area of the trophoblast cells (**Fig. 2l**, WT; **m,n**, Pat-KO). These results indicate that a phagocytic reaction to the endothelial cells was induced in the surrounding layer III trophoblast cells. Thus, the resulting placental infarction seems to cause placental malfunction, such as incomplete material transport between the maternal and the fetal blood, presumably leading to the late-fetal growth retardation and lethality in the Pat-KO fetuses.

We confirmed functional deficiency of the Pat-KO placenta by nutrition transfer assay[10,11]. We examined both active and passive transport at 15.5 d.p.c. using two radiolabeled substrates, [^{14}C]methylaminoisobutyric acid (Me-AIB) and [^{14}C]inulin, respectively. We did not find any significant difference between WT and Pat-KO placentas in materno-fetal transfer of [^{14}C]Me-AIB, a non-metabolizable amino acid analog, through the System A amino acid transport system ($P = 0.158$; **Fig. 3a**). However, the passive permeability of inulin was significantly lower in Pat-KO placenta (48% compared with WT, $P = 0.000123$; **Fig. 3b**), indicating that Rtl1 deficiency had damaged the placental physical barrier but had not affected the active transport system[12]. In the case of Mat-KO, placentomegaly was associated with expansion of the inner spaces of the fetal capillaries (**Fig. 1h** and **Fig. 2o**, WT; **p**, Mat-KO, and **q**). The most severe abnormalities were found in the surrounding layer III trophoblast cells, which showed a large number of vacuoles, indicating that these cells were starving (**Fig. 2r**, WT; **s,t**, Mat-KO).

IHC staining with antibody to Rtl1 showed that Rtl1 protein localized exclusively in the labyrinth zone at 18.5 d.p.c.; no signals in the other layers of the placenta were observed (**Fig. 4a–d**). Co-immunostaining with CD31 showed that Rtl1 localized around the nuclei of the capillary endothelial cells, where anomalies in both Pat-KO and Mat-KO were observed (**Fig. 4e**). We did not observe any signals in the Pat-KO placentas, but we observed strong signals in the

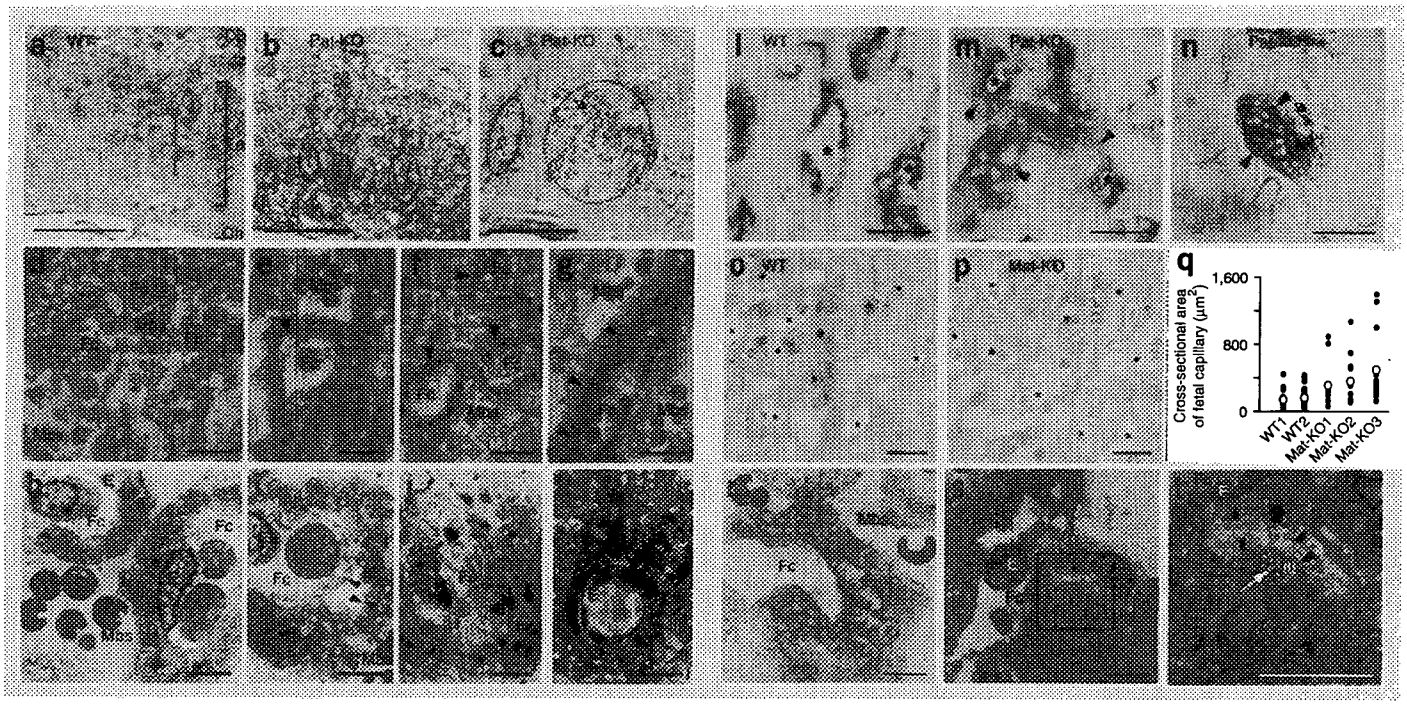

Figure 2 Histological abnormalities observed in day 15.5 Pat-KO placentas and in day 18.5 Mat-KO placentas. Most abnormalities were observed near the endothelial cells and the surrounding layer III trophoblast of the fetal capillaries in the labyrinth zone. (**a–n**) The labyrinth zone of WT placentas at 15.5 d.p.c. is shown in **a**, **d**, **h** and **l** and that of Pat-KO placentas at the same stage is shown in **b**, **c**, **e–g**, **i–k**, **m** and **n**. (**o–s**) The labyrinth zone of WT placenta at 18.5 d.p.c. is shown in **o** and **r**, and that of the Mat-KO placenta at the same stage is shown in **p** and **s**. H&E staining in **a–c**; scale bar, 0.5 mm. Truidin blue staining in **d–g**,**o** and **p**; scale bar, 10 μm for **d–g**, 20 μm for **o** and **p**. The arrowheads indicate an abnormal space between the endothelial cell and the layer III trophoblast in **e**, abnormally appearing lysosomes in **f** and a clogged fetal capillary in **g**. Clogging, as seen in **g** and **k**, was found mainly in the dark-stained regions, as shown in the dotted circles in **b** and **c**. Electron microscopy images in **h–k**,**r** and **s**; scale bar, 5 μm. The arrowheads indicate an abnormal space between the endothelial cell and the layer III trophoblast in **i**. (**t**) Magnified figure of the square area in **s**; scale bar, 5 μm. The black arrowheads indicate an abnormal space between the endothelial cell and the layer III trophoblast, and the white arrow indicates vacuoles in the layer III trophoblast. IHC staining in **l–n** with antibody to CD31; scale bar, 20 μm. The arrowheads indicate an abnormally diffused signal of endothelial cell marker in **m** and a disrupted fetal capillary in **n**. The same result was obtained with an antibody to CD34, another endothelial specific marker (data not shown). **q** shows a cross-sectional area of fetal capillary that was measured using ImageJ. The Pat-KO fetus associated with placenta **c** and **n** was already dead at 15.5 d.p.c. At present, it remains unclear whether the neonatal lethal phenotypes in both Pat-KO and Mat-KO are primarily due to direct or indirect effects of the severe placental anomalies, although both are likely to be involved. Further investigation will be necessary to reveal whether there is a specific cause for neonatal lethality. Db, decidua basalis; Jz, junctional zone; Lz, labyrinth zone; Ch, chorionic plate; Mbs, maternal blood sinus; Fc, fetal capillary; E, endothelial cell; I/II/III, layer I/II/III trophoblast. The asterisks in **l–p** indicate fetal capillaries.

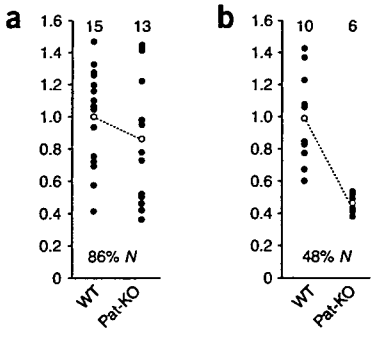

Figure 3 Placental transfer assay. (**a**) Placental transfer of [^{14}C]Me-AIB at 15.5 d.p.c. (**b**) Placental transfer of [^{14}C]inulin at 15.5 d.p.c. Each substrate was injected from the jugular vein of pregnant females at 15.5 d.p.c., and the amount of the labeled substances that entered the fetus through the placenta was determined 3–4 min after injection[10,11]. The fetal accumulation of radioisotope per milligram of placenta was calculated and compared between WT and Pat-KO. The average of WT in every littermate was defined as 1. No significant difference in the active transfer of Me-AIB between WT and Pat-KO placenta was found (86%, $P = 0.158$). However, the passive permeability of inulin in Pat-KO was decreased to about 50% of that in WT (48%, $P = 0.000123$).

Mat-KO placentas, as expected (**Fig. 4f,g**; see also **Supplementary Fig. 4** online). No Rtl1 protein was detected in the endothelial cells of the umbilical cord, although they are connected to the fetal capillaries and are of the same origin as placental endothelial cells (**Fig. 4a,d**). Therefore, we concluded that Rtl1 functions exclusively in the placental endothelial cells for the maintenance of the feto-maternal interface during late-fetal development. To create the novel feto-maternal interface in the course of evolution, the endothelial cells may need a unique protein to regulate the trophoblast cells that have intrinsically invasive and phagocytotic features.

These experiments demonstrate that among several candidate imprinted genes, *Rtl1* is one of the major genes responsible for maternal and paternal duplication of distal chromosome 12 (PatDp (dist12) and MatDp(dist12)) as well as for the corresponding uniparental disomies (MatDi(12) and PatDi(12))[4–6] (**Supplementary Table 1**). The MatDp(dist12) phenotypes of late-fetal and neonatal lethality associated with intrauterine growth retardation are consistent with those of *Rtl1* Pat-KO. *Dlk1* Pat-KO and *Dio3* null mice also showed reduced neonatal size and viability to a certain degree, but this did not account for the severe lethality of MatDp(dist12) and MatDi(12)[13,14]. Therefore, we conclude that the loss of *Rtl1* expression has an important role in such late-fetal viability and that *Dlk1*, *Rtl1* and possibly *Dio3* can independently contribute to late-fetal growth and neonatal lethality. *Rtl1* Mat-KO mice show notable overgrowth and morphological abnormalities of the placenta consistent with the PatDi(12) mice phenotypes[15]. The Mat-KO mice show only a 2.5- to 3.0-fold increment of *Rtl1* from a single normal paternal allele as a result of the lack of *Rtl1as* from the maternal allele. Therefore, an approximately 4.5-fold overexpression of *Rtl1* from the two paternal alleles that would be expected in PatDi(12) and PatDp(dist12) mice[9] may explain their late-fetal lethality, rather than the neonatal lethality in the Mat-KO.

Rtl1 is one of 11 retrotransposon-derived genes related to the sushi-ichi retrotransposon that are specifically conserved in eutherian mammals[16–20]. Eutherian orthologs of *Rtl1* have a high degree of amino acid conservation and low synonymous-to-nonsynonymous substitution rates (dN/dS), supporting the claim that *Rtl1* has a common and crucially important function in the placenta among eutherians, including human beings[17,21] (**Supplementary Fig. 5** online). This work provides evidence for exaptation, the acquisition

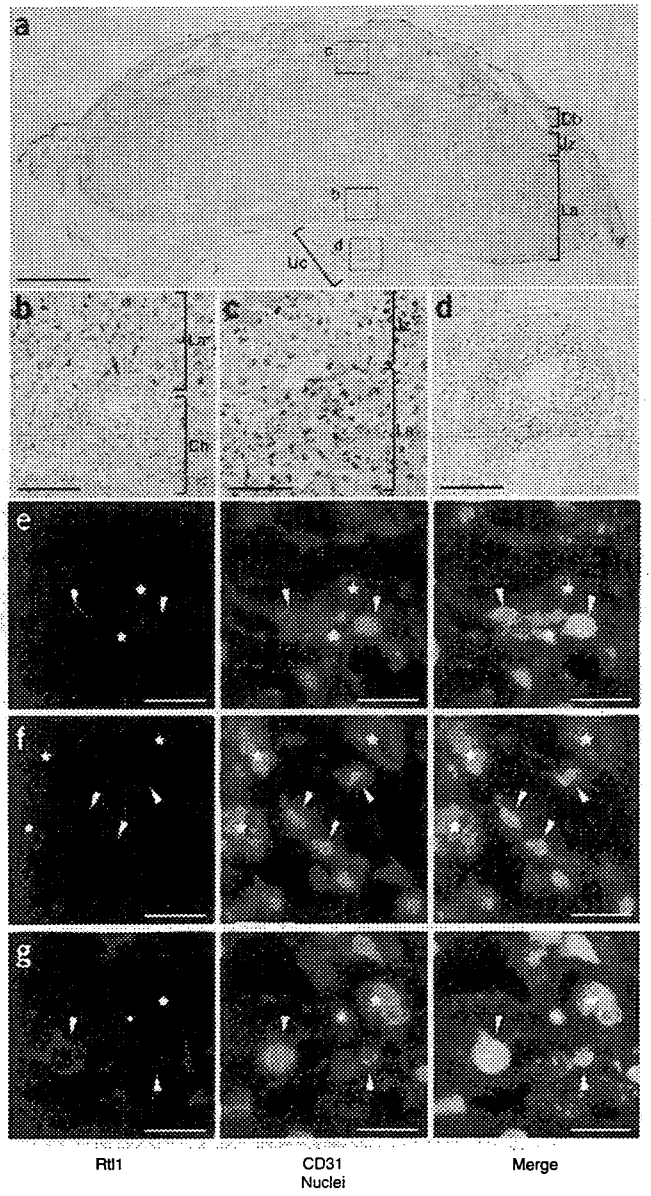

Figure 4 Rtl1 protein localization in the placentas at 18.5 d.p.c. by immunohistochemistry. (**a–c**) Whole placenta image (**a**) and its magnified images (indicated as each small square) of the boundary regions of the placental zones between the labyrinth zone (La) and chorionic plate (Ch) (**b**) and between La and the junctional zone (Jz) (**c**). (**d**) Umbilical cord (Uc) connecting to the fetal capillaries. The signals of Rtl1 (brown by DAB staining) are seen exclusively in La but not in Ch, Jz, decidual basalis (Db) or Uc. Scale bar, 1 mm for **a** and 100 μm for **b–d**. (**e–g**) Co-immunostaining of Rtl1 (red, left), CD31 and nuclei (green and blue, respectively, middle) and their merged image (right). The labyrinth zones of WT (**e**), Pat-KO (**f**) and Mat-KO (**g**) are shown. The arrowheads and stars indicate nuclei of endothelial cells and trophoblast cells, respectively. Scale bar, 20 μm. Only the perinuclear region in the endothelial cells were stained by antibody to Rtl1 in WT (**e**) and Mat-KO (**g**). Note that the inner areas of the endothelial cells were also stained when Rtl1 was overproduced in Mat-KO (**g**; left and right).